NASA Technical Memorandum 80072

ONSET OF CONDENSATION EFFECTS AS DETECTED BY
TOTAL PRESSURE PROBES IN THE LANGLEY 0.3-METER
TRANSONIC CRYOGENIC TUNNEL

ROBERT M. HALL

MAY 1979

1 Report No NASA TM-80072	2 Government Accession No	3 Recipient's Catalog No
4 Title and Subtitle ONSET OF CONDENSATION EFFECTS AS DETECTED BY TOTAL PRESSURE PROBES IN THE LANGLEY 0.3-METER TRANSONIC CRYOGENIC TUNNEL		5 Report Date May 1979
		6 Performing Organization Code
7 Author(s) Robert M. Hall		8 Performing Organization Report No
9 Performing Organization Name and Address NASA Langley Research Center Hampton, Virginia 23665		10 Work Unit No 505-06-43-08
		11 Contract or Grant No
12 Sponsoring Agency Name and Address National Aeronautics and Space Administration Washington, DC 20546		13 Type of Report and Period Covered Technical Memorandum
		14 Sponsoring Agency Code

15 Supplementary Notes

16 Abstract

Total pressure probes mounted in the test section of the Langley 0.3-meter transonic cryogenic tunnel are used to detect the onset of condensation effects for free-stream Mach numbers of 0.50, 0.75, 0.85, and 0.95 and for total pressures between one and five atmospheres. The amount of supercooling is found to be about 3 K and suggests that condensation is occurring on pre-existing liquid nitrogen droplets resulting from incomplete evaporation of the liquid nitrogen injected to cool the tunnel. The liquid nitrogen injection process presently being used for the 0.3-m tunnel results in a wide spectrum of droplet sizes being injected into the flow. Since the relatively larger droplets take much more time to evaporate than the more numerous smaller droplets, the larger ones reach the test section first as the tunnel operating temperature is reduced. However, condensation effects in the test section are not immediately measurable because there is not a sufficient number of the larger droplets to have an influence on the thermodynamics of the flow.

17 Key Words (Suggested by Author(s)) Condensation Cryogenic wind tunnels Minimum operating temperatures	18 Distribution Statement Star Category - 02 Unclassified - Unlimited		
19 Security Classif (of this report) Unclassified	20 Security Classif (of this page) Unclassified	21 No of Pages 51	22 Price* $5.25

ONSET OF CONDENSATION EFFECTS AS DETECTED BY TOTAL PRESSURE PROBES IN THE LANGLEY 0.3-METER TRANSONIC CRYOGENIC TUNNEL

Robert M. Hall

NASA Langley Research Center
Hampton, Virginia 23665

SUMMARY

Total pressure probes mounted in the test section of the Langley 0.3-meter transonic cryogenic tunnel are used to detect the onset of condensation effects for free-stream Mach numbers of 0.50, 0.75, 0.85, and 0.95 and for total pressures between one and five atmospheres. The amount of super-cooling is found to be about 3 K and suggests that condensation is occurring on pre-existing liquid nitrogen droplets resulting from incomplete evaporation of the liquid nitrogen injected to cool the tunnel. The liquid nitrogen injection process presently being used for the 0.3-m tunnel results in a wide spectrum of droplet sizes being injected into the flow. Since the relatively larger droplets take much more time to evaporate than the more numerous smaller droplets, the larger ones reach the test section first as the tunnel operating temperature is reduced. However, condensation effects in the test section are not immediately measurable because there is not a sufficient number of the larger droplets to have an influence on the thermodynamics of the flow.

INTRODUCTION

The lower the operating temperature of nitrogen-gas, transonic cryo-
genic wind tunnels, the greater the benefits of cryogenic operation such
as increased unit Reynolds number and reduced drive power for a given
tunnel operating pressure. As explained in references 1 and 2, the
lower temperature limit of useful operation is determined by the
onset of condensation effects. As a part of the on-going effort at the
Langley Research Center to investigate the minimum operating temperatures
of cryogenic wind tunnels, condensation data have been taken using
total pressure probes mounted at positions of 0.33, 0.49, 0.65, and
0.81-m downstream of the entrance of the test section of the Langley 0.3-meter
transonic cryogenic tunnel. The total temperatures at which the onset of con-
densation effects on these probes occurred was measured at Mach numbers between
0.50 and 0.95 and at tunnel total pressures between 1 and 5 atmospheres.
The dual objectives of this test were to detect the onset of condensation
effects occurring in the test section and to determine the influence of
length on the magnitude of effects.

SYMBOLS

b constant defined by equation (8), m^{-1}

C_p pressure coefficient, $\dfrac{p - p_\infty}{q_\infty}$

ΔC_p difference in C_p defined by equation (1)

d_o injection orifice diameter, m

D   diameter of droplet, m (unless otherwise noted)

D_{32} volume to surface ratio for mean droplet diameter, m (unless otherwise noted)

L   latent heat, J/kg

M   Mach number

n   total number of droplets injected per second

Δn number of droplets injected per second in a given size range

p   pressure, atm (1 atm = 101325 N/m^2)

q   dynamic pressure, atm

r   droplet radius, m

R   Reynolds number per meter

t   time, sec

T   temperature, K

ΔT supercooling defined by equation (5), K

V   velocity, m/sec

x   distance downstream of the beginning of the test section, m

λ thermal conductivity, J/(m·K·sec)

μ viscosity, kg/(m·sec)

ρ density, kg/m^3

σ surface tension, N/m

$\bar{\sigma}$ standard deviation in temperature, K

Subscripts

cor   corrected value

e   conditions at onset of condensation effects

f   conditions at final time

i   conditions at initial time

3

inj	conditions at the injection station
ℓ	pertaining to liquid
s	conditions at the intersection of isentrope and vapor pressure curve
t	pertaining to total conditions
v	pertaining to vapor
∞	pertaining to free-stream conditions

EXPERIMENTAL APPARATUS

Tunnel

The Langley 0.3-m transonic cryogenic tunnel is a continuous flow, fan-driven tunnel, which uses nitrogen as a test gas and is cooled by injecting liquid nitrogen directly into the stream. For these total pressure probe tests, the total temperature was varied from 80 to 103 K, while the total pressure was varied from 1.2 to 4.7 atm. Some of the design features and operational characteristics of the 0.3-m tunnel are reported by Kilgore in reference 3, and a sketch of the tunnel is shown in figure 1.

The liquid nitrogen used to cool down the tunnel structure and absorb the heat added to the stream by the drive fan was injected into the tunnel for the present tests through eleven nozzles arranged on three struts, or spray bars, at the three injection stations shown in figure 1. Full details of this arrangement are included in reference 3.

Examples of the total temperature distribution in the reservoir section are given in figure 2. As seen in this figure, the standard deviation in total temperature, $\bar{\sigma}$, can be as large as 1 K.

Probes

The placement of the four total pressure probes at various positions around the outer portions of the test section is shown in figure 3. The legend on the lower right of the figure gives the distances downstream from the beginning of the test section while the sketch on the right shows the dimensions of the probes. The pressures are measured by a scanning pressure valve, whose reference pressure was the tunnel reservoir total pressure.

Error Discussion

Uncertainty in the value of pressure coefficient, C_p, calculated for each probe may be the result of at least three influences: fluctuations in tunnel Mach number, M_∞; fluctuations in tunnel total pressure, p_t; and uncertainties in total temperature, T_t, that arise both from differences in T_t over the cross section of the tunnel as well as fluctuations in T_t for the tunnel as a whole. Concerning the first influence, if M_∞ changes between the time the tunnel static pressure is recorded and the time at which the total pressure is recorded, an incorrect value of dynamic pressure will be used in the calculation of C_p and an error will result. As mentioned in reference 2, the Mach number in the 0.3-meter tunnel fluctuates by approximately ± 0.003, and this is the value used in the calculations to follow.

5

In order to minimize the effect of the second influence - fluctuations in p_t - the stagnation pressure measured in the settling chamber of the tunnel was taken to be the reference pressure on the scanning pressure value. Except for any possible high frequency fluctuations in the tunnel, this arrangement should have minimized any effects of total pressure fluctuations because the scanning value was measuring only differences in total pressure between the reservoir and the test section. Furthermore, by measuring only differences in p_t, the test could be made with a more sensitive 0.68 atm transducer in the scanning value.

The uncertainty in total temperature, the third influence, arises primarily from the total temperature variation over the cross section of the tunnel, as seen in figure 2. As mentioned earlier, the standard deviation for these differences in T_t over the cross section is approximately 1 K. Another uncertainty in total temperature arises as a result of fluctuations in the magnitude of T_t for the tunnel as a whole. The magnitude of this second uncertainty in T_t is estimated to be 0.5 K over the data acquisition period. However, since the second uncertainty is half the magnitude of the first, the uncertainty in T_t for each probe is taken to be the magnitude of the variations in T_t over the cross section, which is 1 K. In summary, any error bars used to represent the uncertainty in C_p or T_t will be based on an uncertainty in M_∞ of ± 0.003, a negligible uncertainty in p_t, and an uncertainty in T_t of ± 1 K.

TESTS

Data Sampled

To determine the total temperature at which effects are seen by the total pressure probes and to investigate the influence of total pressure and free-stream Mach number on the onset of condensation effects, the

tunnel was operated at free-stream Mach numbers of 0.50, 0.75, 0.85, and 0.95 over a total pressure range of 1.2 to 5.0 atm. For each of the four values of M_∞, test envelopes were drawn which covered those tunnel p_t and T_t ranges that were of interest and that were obtainable in the 0.3-m tunnel. The envelopes were bounded in p_t by the 1.2 to 5.0 atm pressure limits and were bounded in T_t by total temperatures above those corresponding to saturation in the test section and bounded below by those corresponding to saturation in the reservoir section.

To explore each test envelope in the p_t and T_t plane, paths of constant unit Reynolds number, R, and M_∞ were used to traverse the region of interest. Since along each of the paths both M_∞ and R were held constant, systematic deviation in pressure coefficients at any probe location was taken to be the result of condensation effects. The paths for the 0.75, 0.85, and 0.95 tests were chosen to span a similar range as the paths in reference 2.

Data Analysis

The primary data analysis tools used consisted of a graphical presentation of the differences in C_p,

$$\Delta C_p = C_p - C_{p,ave} , \qquad (1)$$

for each total pressure probe as a function of total temperature, where $C_{p,ave}$ is the average value of C_p for a given total pressure probe before the onset of effects. Some of the data was taken with known differences of ± 0.005 between the desired and the achieved Mach number. In order to reduce the scatter in ΔC_p due to this effect, a Mach number correction was used.

7

Of course, this correction procedure only deals with known differences

in M_∞ recorded as the data was taken and does not change any

error estimate for C_p due to random fluctuations in M_∞ between the time

the tunnel conditions were recorded and the time that the pressure at the

total pressure probe was recorded.

The first step in the Mach number correction procedure is to assume isentropic flow and that nitrogen is a perfect gas with a ratio of specific heats equal to 1.4. Then C_p can be easily written as a function of M_∞ for a total pressure probe as follows

$$C_p = \frac{(1 + .2M_\infty^2)^{3.5} - 1}{.7M_\infty^2} \tag{2}$$

(Comparisons of full real-gas, isentropic flow analyses to ideal-gas expressions such as equation (2) have shown insignificant differences between results, so using ideal-gas equations for the correction process is very satisfactory.) The derivative of C_p can be written as

$$\frac{dC_p}{dM_\infty} = \frac{1.4 \, M_\infty^2 (1 + .2M_\infty^2)^{2.5} - 2[(1 + .2M_\infty^2)^{3.5} - 1]}{.7 \, M_\infty^3} \tag{3}$$

Equation 3 is then used to obtain corrected values of C_p by averaging all the nominally constant Mach numbers along a given path to find a specific value of M_∞, called $M_{\infty,cor}$. All the values of C_p for that path are then normalized to $M_{\infty,cor}$ by the following equation

8

$$C_{p,cor} = C_p + \frac{dC_p}{dM_\infty} (M_{\infty,cor} - M_\infty) \tag{4}$$

where $C_{p,cor}$ is the value of C_p corrected from M_∞ to $M_{\infty,cor}$.

RESULTS

The data taken will now be summarized by groups of figures for each of the four values of M_∞: 0.50, 0.75, 0.85, and 0.95. In each group the first figure shows the paths of constant unit Reynolds number, R, and nominally constant M_∞ as well as the pertinent saturation boundaries. For each path, a figure is shown of the differences in C_p as measured by each total pressure probe as a function of total temperature. Above the free-stream saturation temperature, there should be little or no effect, but below this temperature the flow is saturated and condensation can occur on any existing seed particles. The last figure in each group shows the total temperature along each path at which effects are first seen as well as the estimation of the uncertainty involved in reading the graphs of differences in C_p.

The lowest Mach number test is for $M_\infty = 0.50$. The paths of constant unit Reynolds number, R, and M_∞ are shown in figure 4 along with the appropriate saturation lines for free-stream as well as reservoir saturation. The graphs of differences in C_p, $C_p - C_{p,ave}$, as a function of total temperature are shown for each path in figures 5 to 8. The error

bar shown to the right of the graphs, if centered over a difference value,
gives the one sigma uncertainty in ΔC_p due to M_∞ fluctuations and
in total temperature due to temperature variation over the cross section.
Also, the total temperatures corresponding to free-stream and reservoir
saturation are labelled under "SAT STAGES" in the figures by the lines
"FS" and "RES", respectively. The values for "PTAVE" shown in the upper
right hand side of the figure represent an average value of the total
pressure (in atmospheres) for the path. For the path described in
figure 5, the onset of condensation effects is shown to be 81.0 K,
but onset is not 100% certain at 80.4 K, which is the minimum temperature
sampled. Consequently, there is no lower bound to the uncertainty for the
value of onset total temperature. In figures 6 and 7 there is no evidence
of onset occurring at all - the upper possible bound of effects is shown at
the minimum temperature at which data was taken. Figure 8 shows, as does
figure 5, possible onset of effects. The summary of the values for onset
total temperature is shown in figure 9. The results for $M_\infty = 0.75$ are
shown in figures 10 to 15. The results for $M_\infty = 0.85$ are shown in figures
16 to 21. At $M_\infty = 0.95$ only two paths of constant R were obtained as
shown in figure 22. The onset graphs are shown in figures 23 and 24 and
the results are summarized in figure 25.

DISCUSSION

Supercooling

A traditional means of comparing and presenting the onset of con-
densation effects is with graphs of supercooling, ΔT, where ΔT is
defined as

10

$$\Delta T = T_s - T_e \tag{5}$$

and T_s is the static temperature at which the flow isentrope crosses the vapor pressure curve and T_e is the static temperature on the same isentrope at which condensation effects are first detected. The onset of condensation effects for the various free-stream Mach numbers will be presented in terms of supercooling and then compared with the results of supercooling from an earlier test of an NACA 0012-64 airfoil. Implications will then be drawn from the amount of supercooling observed.

As seen in figure 26 for the total pressure probes, the magnitude of supercooling calculated using stream static temperature as T_e in equation (5) remains approximately constant at 3 K and does not seem to depend strongly on either tunnel pressure or free-stream Mach number. A similar conclusion concerning the importance of free-stream static temperature is found in reference 2, which describes tests in the Langley 0.3-meter tunnel on a NACA 0012-64 airfoil. In the analysis of that experiment, T_e is taken to be either the static temperature in the region of highest local Mach number over the airfoil or the free-stream static temperature. The former case is shown in figure 27 and the latter case is shown in figure 28. Clearly, the supercooling data collapse to a constant value when the free-stream static temperature is used to calculate the values of supercooling. Furthermore, the magnitude of supercooling based on free-stream static temperature - between 2 and 3 K - is very similar in magnitude to the values of supercooling found in the present total pressure probe experiments. The similarity of figures 26 and 28 strongly suggests that the condensation effects are occurring in the free-stream flow and are independent of the presence of the total pressure probes or the airfoil.

11

That the effects are linked with the free-stream flow should help determine
the mode of nucleation causing the condensation. Homogeneous nucleation
occurs when the gas has been sufficiently cooled below the saturation tempera-
ture to enable the gas molecules to overcome the surface energy **barrier** to drop-
let formation (see reference 4 for details). Heterogeneous nucleation occurs
when there are pre-existing seed particles in the flow upon which gas molecules
can condense as soon as the gas temperature drops below the saturation tempera-
ture. As noted by Sivier in **reference 5,** either or both nucleation
processes can occur. The governing factor is the number of
seed particles present and the size of the particles. If there
are enough seed particles present to allow sufficient condensation to heat the
remaining gas, then the gas may never become cool enough to overcome the sur-
face energy barrier to droplet formation. On the other hand, if there is an
insufficient number of seed particles to influence the thermodynamics of the
flow and if there is sufficient cooling below the saturation temperature to
overcome the energy barrier to droplet formation, then homogeneous nucleation
can take place.

In the present total pressure experiments as well as in the airfoil tests,
the fact that effects are seen with only about 3 K of supercooling in the free
stream implies that heterogeneous nucleation is occurring because much higher
values of supercooling have been previously observed both in experimental data
and in theoretical work as discussed in reference 5. For example, by fitting
a curve to the onset temperatures for homogeneous nucleation as predicted by
Sivier, Adcock of Langley Research Center arrived at the following equation
for T_e, static temperature at the onset of condensation effects, as

$$\frac{1}{T_e} = 1.461 \times 10^{-2} - 4.962 \times 10^{-3} \times \log_{10} p + 1.959 \times 10^{-4} \times (\log_{10} p)^2 \tag{6}$$

For the test conditions shown in figure 26, the curve

fit of Adcock would predict a range of supercooling before the onset

of homogeneous nucleation from 16 K at 1 atm to 11 K at 5 atm for the

M_∞ = 0.50 test and a range of supercooling from 17 K at 1 atm to 9 K at

5 atm for the M_∞ = 0.95 test. These magnitudes of supercooling are not seen in

the data and the trend of relatively constant supercooling over the pressure

range is not consistent with the trend of decreasing supercooling with in-

creasing pressure that is associated with homogeneous nucleation. Furthermore,

during the airfoil experiments of reference 2, the apparent correlation between

the onset of condensation effects and the free stream conditions imply that

pre-existing seed particles are causing the observed condensation. As

explained earlier, homogeneous nucleation depends on overcoming an energy

barrier to droplet formation. This energy barrier would be overcome in the

region of maximum local Mach number over the airfoil before it is overcome

in the free stream. Since effects are not detected in this local region over

the airfoil before they are seen over the airfoil as a whole, it again does

not appear that homogeneous nucleation is consistent with the observations.

In summary, the onset of effects for both the total pressure probe tests

reported herein and the airfoil tests of reference 2 appears to be the result of

pre-existing seed particles causing heterogeneous nucleation.

Source of the Seed Particles

The source of the seed particles is incomplete evaporation of the

liquid nitrogen injected for cooling the tunnel. As explained in reference 3,

the liquid is injected into the 0.3-meter tunnel through spray nozzles.

The nozzles break up the liquid into droplets as they

pass into the tunnel perpendicular to the flow. Then, depending

13

on the shear velocity of the stream and on the liquid properties, further aerodynamic break up can occur, as explained in reference 6. After this initial phase, the droplets are moving at approximately the same velocity as the gas and any further reduction in size must come as the result of evaporation of the droplet. At some low temperature, however, there is insufficient temperature difference between the droplets and the stream to evaporate the droplets before they reach the test section. As an example of the droplet evaporation situation, a theoretical droplet distribution due to Nukiyama and Tanasawa (see reference 7) will be applied to cryogenic tunnel conditions typical of the onset of condensation effects and will be combined with a droplet evaporation rate equation to give some insight into the droplet evaporation process.

In 1938 Nukiyama and Tanasawa published a series of reports on droplet atomization. By analyzing empirical results, they were able to formulate expressions to predict the volume to surface mean droplet diameter, D_{32}, and a size distribution about that mean. Their formula for D_{32} is given by

$$D_{32} = \frac{585}{V_v} \sqrt{\frac{\sigma_\ell}{\rho_\ell}} + 597 \left(\frac{\mu_\ell}{\sqrt{\sigma_\ell \rho_\ell}} \right)^{0.45} \left(1000 \frac{Q_\ell}{Q_v} \right)^{1.5} \qquad (7)$$

where D_{32} is in microns; V_v is vapor velocity in m/sec; σ_ℓ, ρ_ℓ, μ_ℓ are the liquid values of surface

14

tension, density, and viscosity in CGS units; and Q_ℓ/Q_v is the ratio of volume of liquid injected to volume of air flowing. For the droplet size distribution function they arrived at the following equation

$$\frac{dn}{n} = 0.5 \; b^3 D^2 \; \exp \; (-bD) \; dD \qquad\qquad (8)$$

where n is the total number of droplets per second and dn is the number of droplets in the size range dD per second. The constant b is empirically found to be

$$b = \frac{5}{D_{32}}. \qquad\qquad (9)$$

In Reference 8, Ingebo and Foster suggest a refinement to equation (8) by placing an empirically determined upper limit to the drop size. Ingebo and Foster use the following expression for the maximum droplet diameter

$$D_{max} = 22.3 \; d_o \; \left(\frac{\sigma_\ell \; \mu_\ell}{\rho_v \rho_\ell \; d_o^2 \; v_v^3} \right)^{0.29} \qquad\qquad (10)$$

where d_o is the diameter of the injection orifice. A typical example

15

of a droplet size distribution calculated for the 0.3-meter tunnel using

equations 7 through 10 is shown in figure 29 for the following conditions:

M_∞ = 0.85, M_{inj} = 0.20, p_t = 4.0 atm, T_t = 96 K, T_L = 80 K, and a percent

of liquid mass injected to mass of air flow of 1.57. The actual numbers

in each size category, Δn, are based on the 3D test section cross-

sectional area of about 0.1 m^2. The liquid temperature, T_L, is taken

to be 80 K during injection because that is the temperature at which the

liquid nitrogen is normally stored and pumped into the tunnel. For

this example D_{32} = 54 x 10^{-6}m and D_{max} = 94 x 10^{-6}m. Both of these

values are very large diameters when compared to typical diameters of

10^{-7} or 10^{-8}m for droplets resulting from homogeneous nucleation.

As a very rough estimate of how long it takes for these droplets

to evaporate, it may be assumed that (1) the droplets evaporate

according to simple continuum growth equations, such as by Oswatitsch

in reference 9, (2) that the vapor and liquid quantities

remain constant during the evaporation process, and (3) the temperature

of the liquid droplets can be taken to be saturation temperature for the

vapor pressure. The droplet growth equation of Oswatitsch can be written

as

$$\frac{dD}{dt} = \frac{4\lambda_v \, (T_\ell - T_v)}{L \, \rho_\ell \, D} \tag{11}$$

16

where D is the droplet diameter in meters. Assuming vapor thermal conductivity, λ_v, droplet temperature, T_ℓ, vapor temperature, T_v, latent heat, L, and liquid density, ρ_ℓ, all remain constant, equation (11) can be integrated over time from an initial diameter, D_1, at t_i to zero diameter at the final time, t_f, to arrive at

$$D_i^2 = \frac{8\lambda_v \ (T_v - T_\ell)(t_f - t_i)}{L \ \rho_\ell} \tag{12}$$

For the example of $p_t = 4.0$ atm and $T_t = 96$ K, values appropriate for equation (12) are

$$T_v = 95.3 \text{ K}$$
$$\lambda_v = .0098 \text{ J/(m·K·sec)}$$
$$L = 1.78 \times 10^5 \text{ J/kg}$$
$$T_\ell = 91.3 \text{ K}$$
$$\rho_\ell = 740 \text{ kg/m}^3$$

where T_ℓ is taken to be the saturation temperature for 4 atms. Substituting these values into equation (12) gives

$$D_i^2 = 2.36 \times 10^{-9} \ (t_f - t_i) \tag{13}$$

17

where D_1 is in meters and t is in seconds. Equation (13) can be used either to approximate the time necessary for the evaporation of a droplet of diameter D_i or to approximate the minimum diameter, D_{min}, that can survive over a certain time interval, $t_f - t_i$. In the 0.3-meter tunnel, the time of flight for a droplet between the primary, #1 injection station and the test section is just over one second; consequently, equation (13) predicts that all droplets of initial diameter larger than about 48×10^{-6}m will reach the test section and that all droplets of smaller diameter will not. This prediction is consistent with the example representing test conditions typical of those at the onset of condensation effects. To examine this more closely, we can consider the conditions of $T_t = 98$ K and $T_t = 94$ K at the same $p_t = 4$ atms. The results for $T_t = 98$ K should show less chance of condensation effects while the results for $T_t = 94$ K should show the potential for much greater effects. To compare all three temperatures, the following table shows the predicted maximum diameter of the droplet, D_{max}, from equation (10), the minimum diameter of droplet, D_{min}, needed for survival to the test section, and n_{min}, the number of droplets per second in the initial distribution that are large enough to survive to the test section.

T_t, K	D_{max},m	D_{min},m	n_{min},sec^{-1}
98	93×10^{-6}	58×10^{-6}	6×10^9
96(onset)	94×10^{-6}	48×10^{-6}	12×10^9
94	96×10^{-6}	34×10^{-6}	40×10^9

If the assumptions used to derive equation (12) are valid and the equation gives a qualitative measure of what is actually occurring, the results shown in the table

18

suggest that there are droplets in the test section before the on-
set of effects are detected although apparently the number are not
sufficient to disturb the total pressure measurements. In fact, the
lack of a clear delineation between the case of no droplets passing through the
test section and no observed effects and the case of many droplets and ob-
served effects may be responsible for the scatter in the values of super-
cooling shown in figure 26.

Some caution, however, is in order in drawing conclusions from the
calculations using equation (12). First, the growth equation,
equation (11), from Oswatitsch assumes there is no convective heating of
the droplet when in reality there will be differences in velocities
between the droplets and the gas. This convective heating will tend to
evaporate the droplet faster than predicted with the Oswatitsch formulation.
Furthermore, the droplet-laden flow encounters four sets of turning vanes
and three turbulence-reducing screens between the liquid nitrogen injection
station and the test section. These obstacles can either reduce or increase the
droplet size distribution because of two competing mechanisms that may be occurring.
First, the injected droplets could wet the turning vanes or screens and lead to much
larger droplets being shed from the trailing edges of the wetted surfaces.
On the other hand, both the turning vanes and the screens will be above
the boiling temperature of the liquid. Consequently, if droplet boiling
occurs upon impact, these obstacles could also lead to a reduction in
droplet size. More study is needed to understand the possible role of these
flow obstacles and more modelling is needed to include convective heating
of the droplets.

19

Effects of Length

One of the original purposes of the experiment was to determine what, if any, effects of length could be expected when extending the results from the 0.3-meter tunnel to a larger tunnel. The present results have been somewhat disappointing in this regard because in figures 8, 12, and 13, for example, the largest effects were not necessarily detected at the probe that was furtherest downstream. Although the anomalies can generally be explained by the uncertainty in total temperature over the cross section of the tunnel, they make detailed analysis difficult. One observation with regard to length effects that is readily apparent from the data is that effects generally appear along the length of the test section at the same total temperature. This conclusion is again consistent with pre-existing droplets entering the test section and causing effects due to vapor condensing on the seed particles. Thus, the length of the test section may not be as important as the size distribution of the droplets entering the test section.

SUMMARY OF RESULTS

Total pressure probes mounted in the test section of the Langley 0.3-meter transonic cryogenic tunnel are used to detect the onset of condensation effects for free-stream Mach numbers between 0.50 and 0.95 and for total pressures between one and five atmospheres. The amount of supercooling is found to be about 3 K and suggests that condensation is occurring on pre-existing liquid nitrogen droplets resulting from incomplete evaporation of the liquid nitrogen injected to cool the tunnel.

The liquid nitrogen injection process results in a large spectrum of droplet sizes being injected into the flow. Since the relatively large droplets take much more time to evaporate than the smaller drops, these larger droplets may reach the test section at a tunnel temperature several degrees Kelvin above the temperature at which effects are detected. However, the small numbers of these larger droplets in the injection spectrum do not appear to be sufficient to influence the thermodynamics of the flow.

Finally, an area outside the scope of this report but important for a full understanding of the droplet evaporation problem is the interaction between the obstacles to the flow – such as the turning vanes and the turbulence screens in the tunnel -- and the size distribution of the droplets. Do these flow obstacles increase or decrease the effective size of the droplets as these obstacles are encountered? More work needs to be done to study this droplet-obstacle interaction.

REFERENCES

1. Adcock, Jerry B.: Real-Gas Effects Associated with One-Dimensional Transonic Flow of Cryogenic Nitrogen. NASA TN D-8274, 1976.

2. Hall, Robert M.: Onset of Condensation Effects with a NACA 0012-64 Airfoil Tested in the Langley 0.3-meter Transonic Cryogenic Tunnel. NASA TP-1385, 1979.

3. Kilgore, Robert A.: Design Features and Operational Characteristics of the Langley Pilot Transonic Cryogenic Tunnel. NASA TM X-72012, 1974.

4. Wegener, P. P.; and Mack, L. M.: Condensation in Supersonic and Hypersonic Wind Tunnels. Advances in Applied Mechanics, Vol. V, 1958, pp. 307-447.

5. Sivier, Kenneth D.: Digital Computer Studies of Condensation in Expanding One-Component Flows. Aerospace Research Laboratories Report ARL 65-234, November 1965.

6. Gooderum, Paul B.; and Bushnell, Dennis M.: Atomization, Drop Size, and Penetration for Cross-Stream Water Injection at High-Altitude Reentry Conditions with Application to the RAM C-I and C-III Flights. NASA TN D-6747, 1972.

7. Nukiyama, Shiro; and Tanasawa, Yasushi (E. Hope, transl.): Experiments on the Atomization of Liquids in an Air Stream. (Reports 1 to 6), Defense Research Board, Canada, 1950.

8. Ingebo, Robert D.; and Foster, Hampton H.: Drop-Size Distribution for Crosscurrent Breakup of Liquid Jets in Airstreams. NASA TN-4087, 1957.

9. Oswatitsch, K. (M. Flint, transl.): Condensation Phenomena in Supersonic Nozzles, Z.A.M.M., vol. 22, no. 1, Feb. 1942, pp. 1-14.
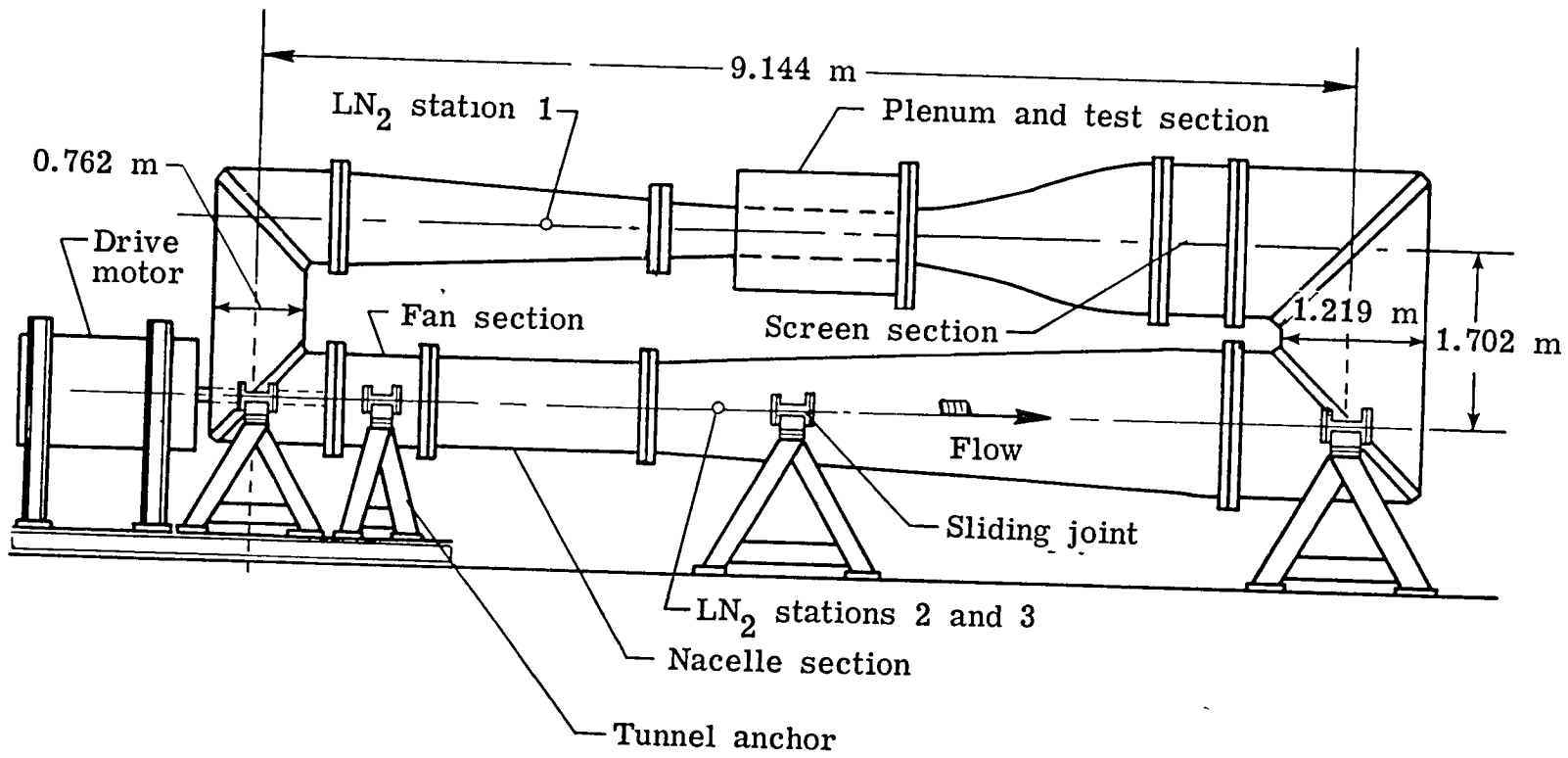
Figure 1.- Schematic of Langley 0.3-m transonic cryogenic tunnel.

$$M_\infty = 0.85$$
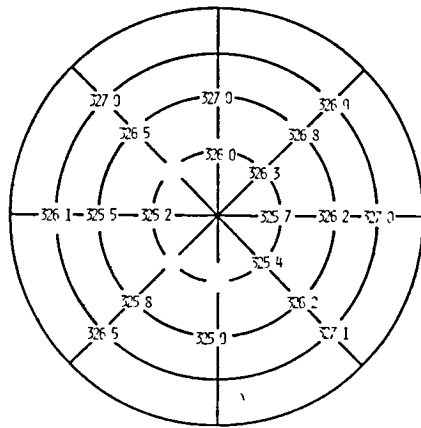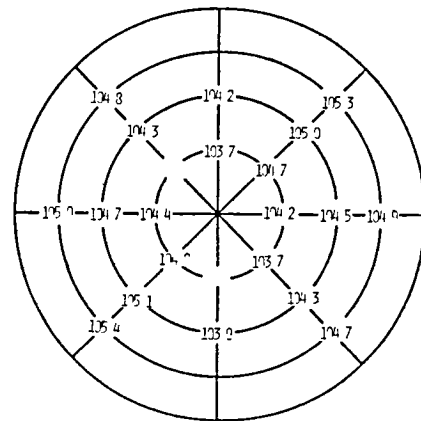
$P_t = 5$ Atm

$T_t = 326.3K, \bar{\sigma} = 0.6K$

$T_t = 104.6K, \bar{\sigma} = 0.5K$

$P_t = 2.5$ Atm.

$T_t = 323.1K, \bar{\sigma} = 1.0K$

$T_t = 116.4K, \bar{\sigma} = 1.0K$

$P_t = 1.2$ Atm.

$T_t = 323.2K, \bar{\sigma} = 0.9K$

$T_t = 89.7K, \bar{\sigma} = 0.6K$
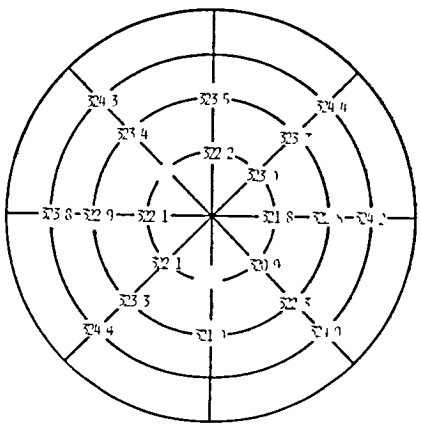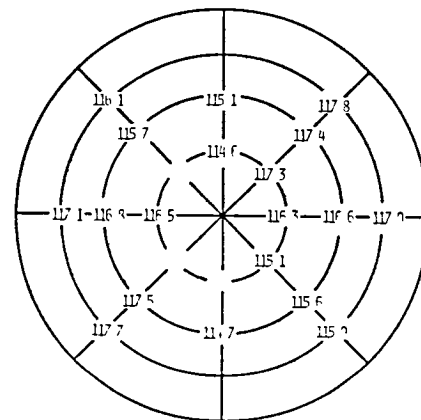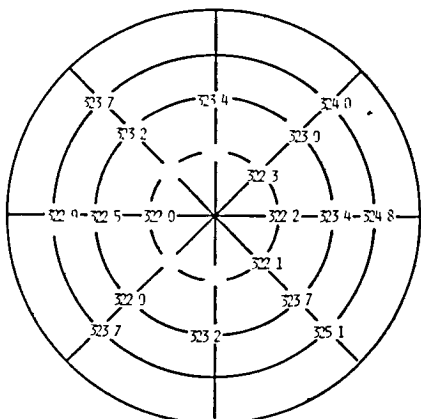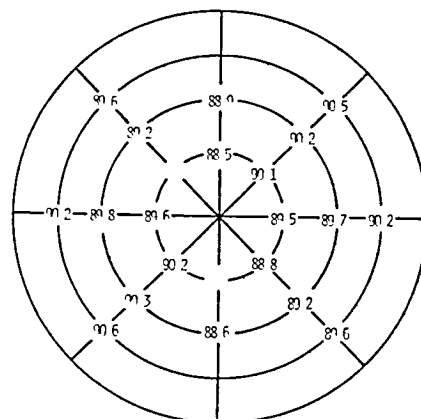
Figure 2.– Examples of transverse temperature distribution in the transonic cryogenic tunnel looking downstream. Measurements made upstream of the screens.
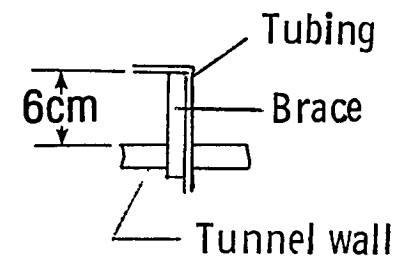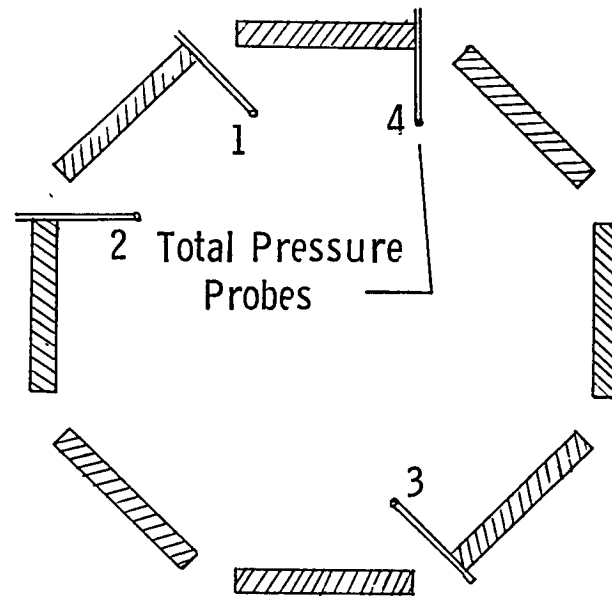
Cross-sectional view of the probes in
the test section looking downstream

Side view of probe

| Probe	Distance downstream
1	0.33m
2	0.49
3	0.65
4	0.81

Figure 3.- Probe placements in the test section.
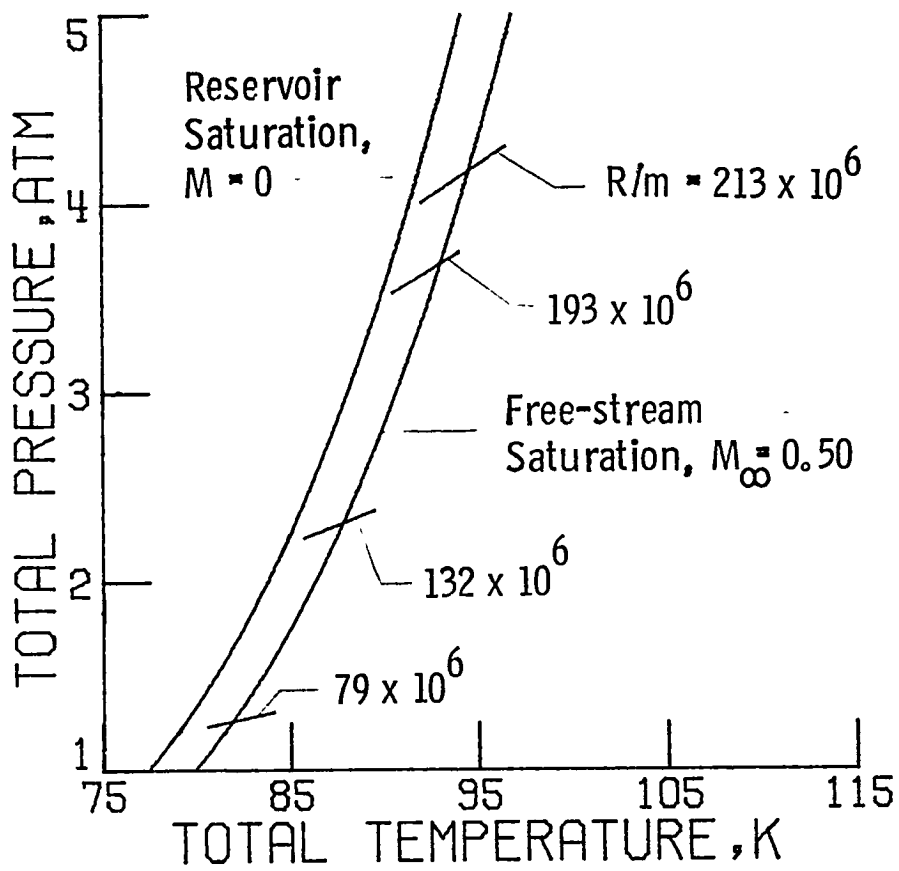
Figure 4.- Paths of constant unit Reynolds number for the $M_\infty = 0.50$ test.
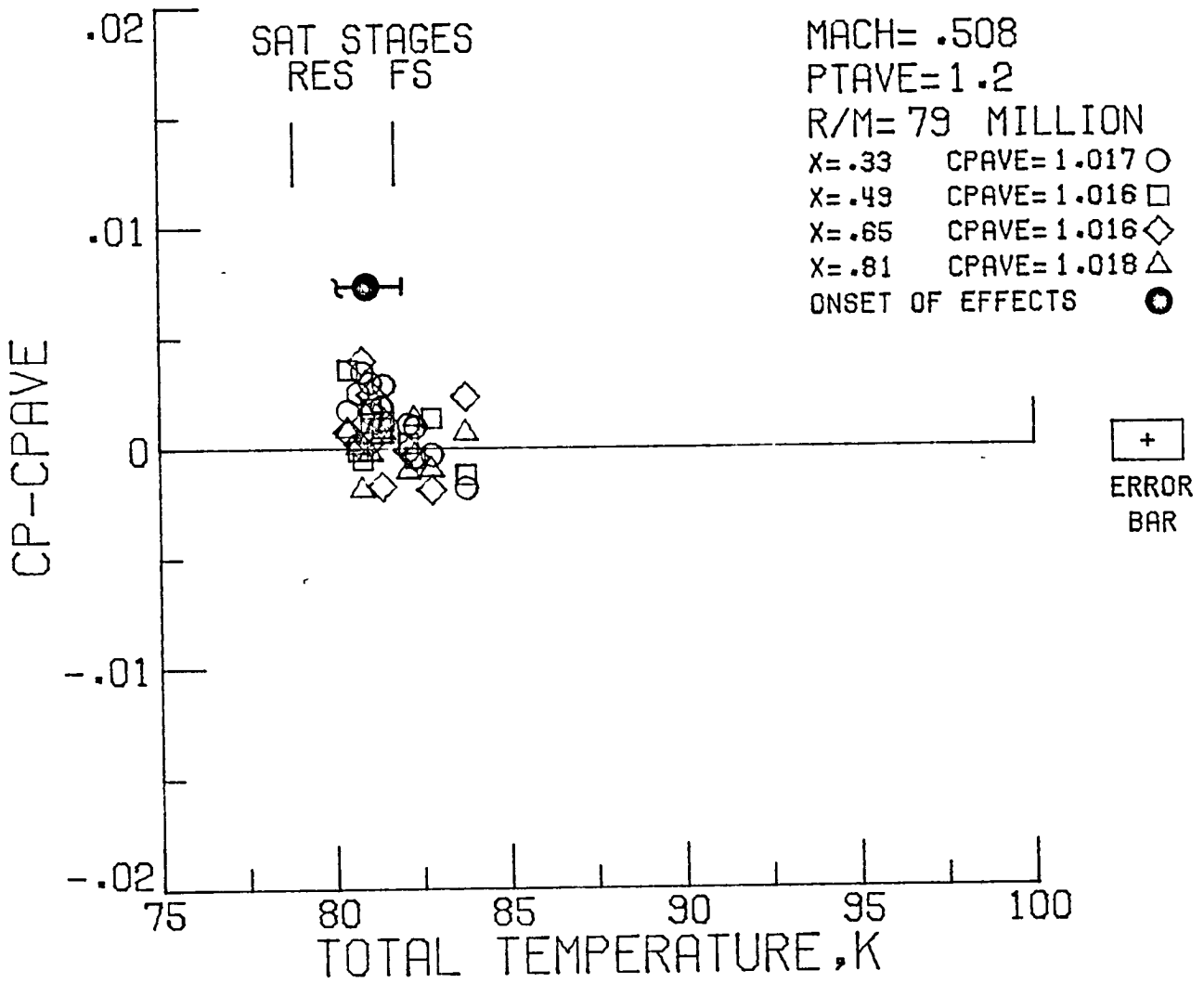
Figure 5.~ Onset of condensation effects for the R/m ~ 79 x 10^{6} path of the M_∞ = 0.50 test.
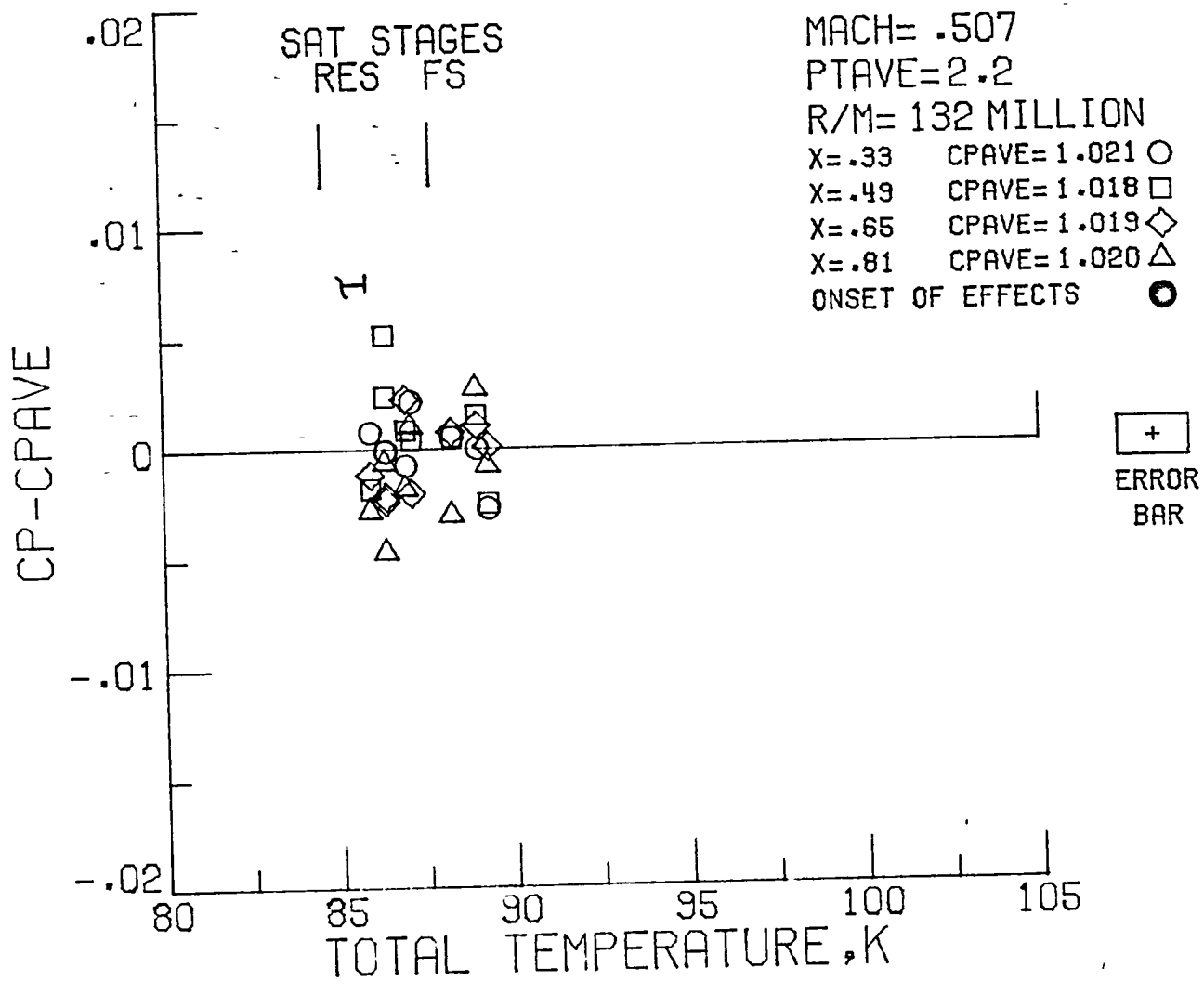
Figure 6. – Onset of condensation effects for the R/m = 132 x 10^6 path of the M$_\infty$ = 0.50 test.
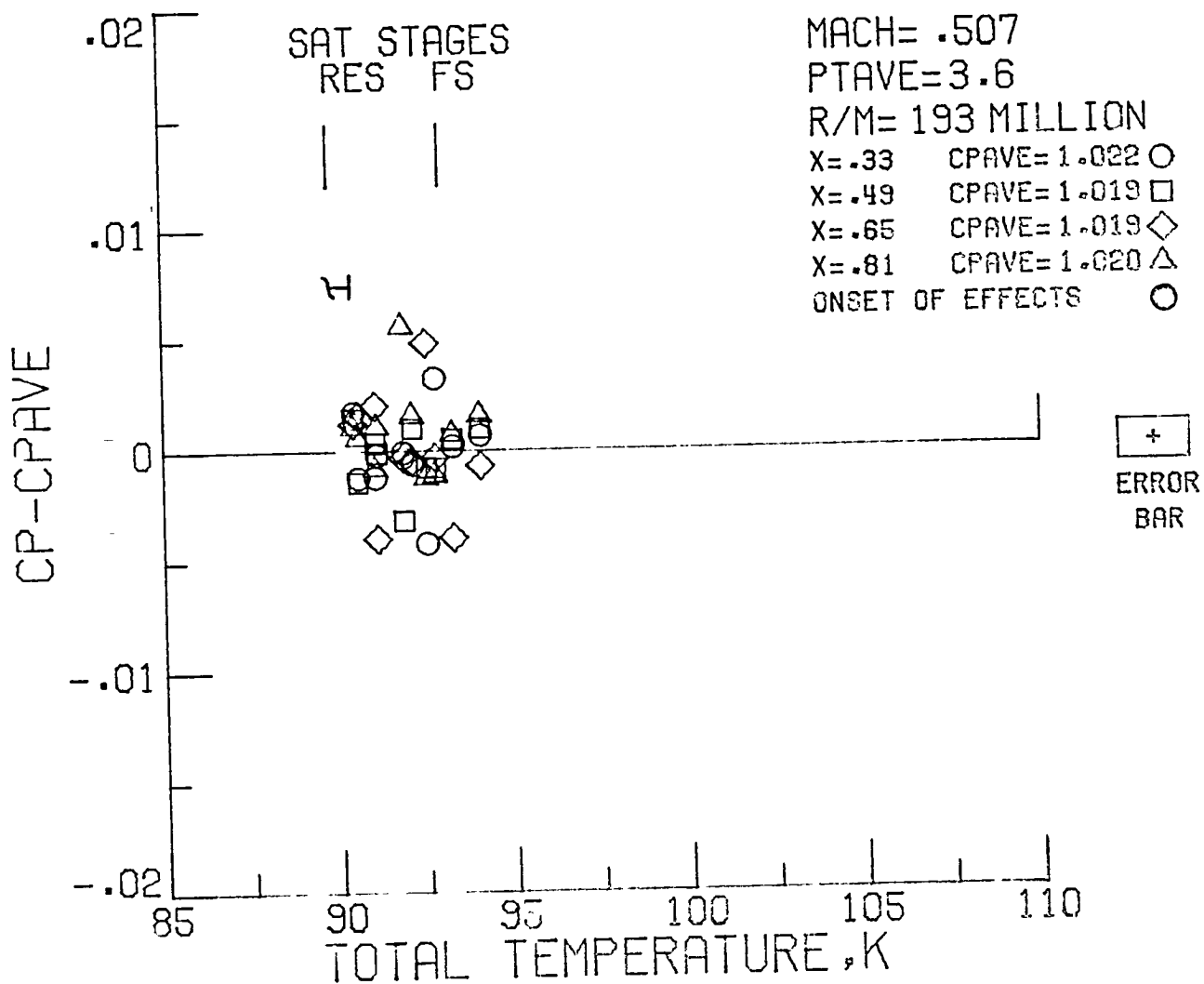
Figure 7.- Onset of condensation effects for the R/m = 193 x 10^6 path of the M$_\infty$ = 0.50 test.
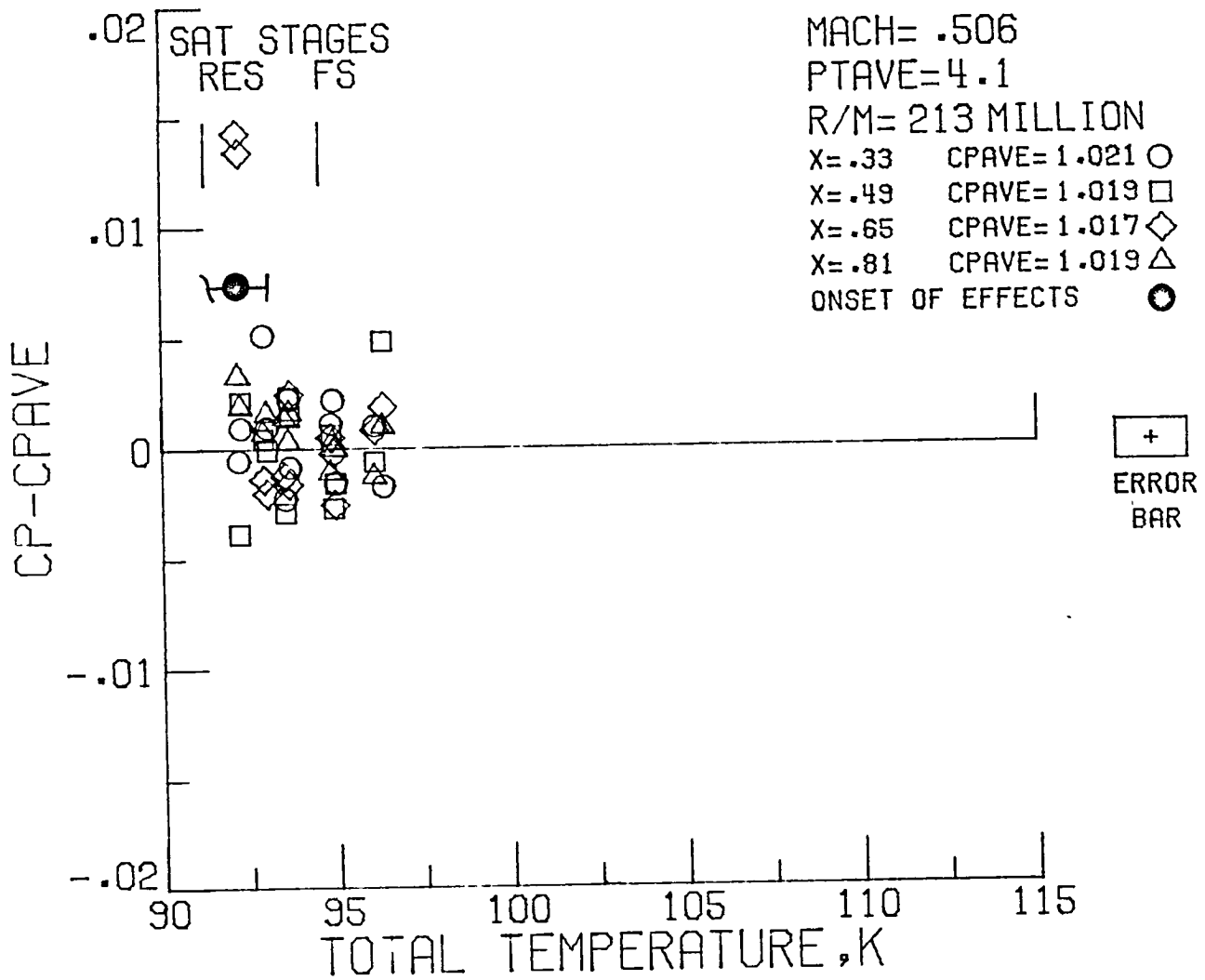
Figure 8.- Onset of condensation effects for the R/m = 213 x 10^6 path of the M$_\infty$ = 0.50 test.
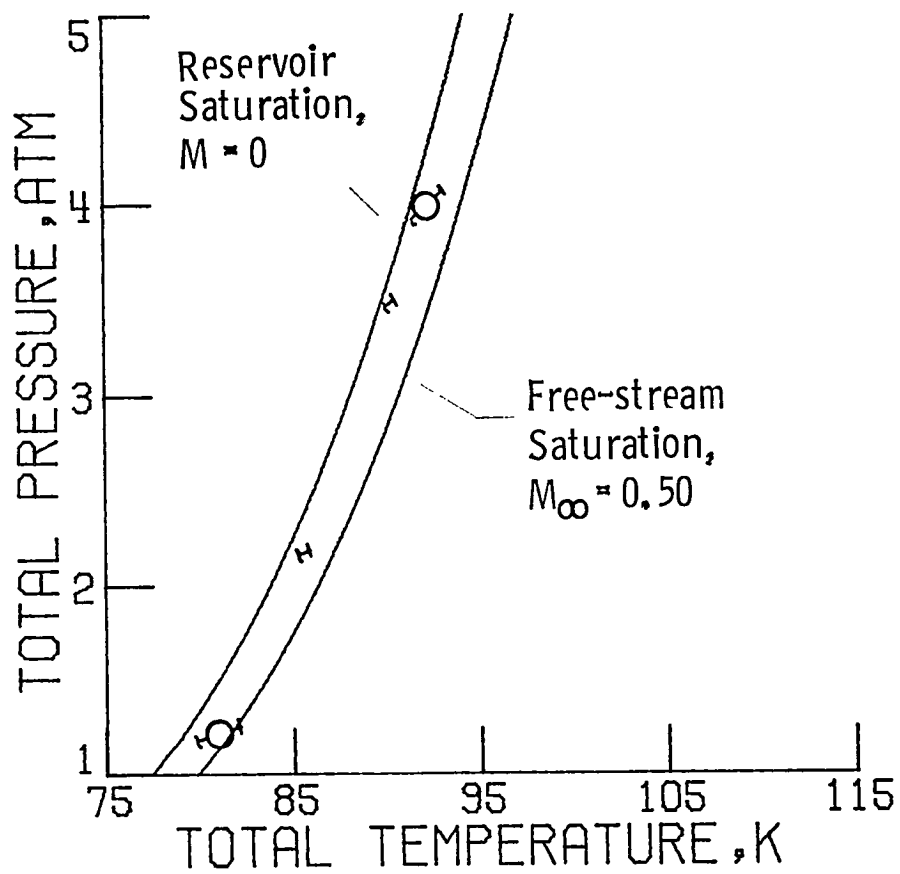
Figure 9.- Summary of the onset of condensation effects and the estimated uncertainties for the M_∞ = 0.50 test.
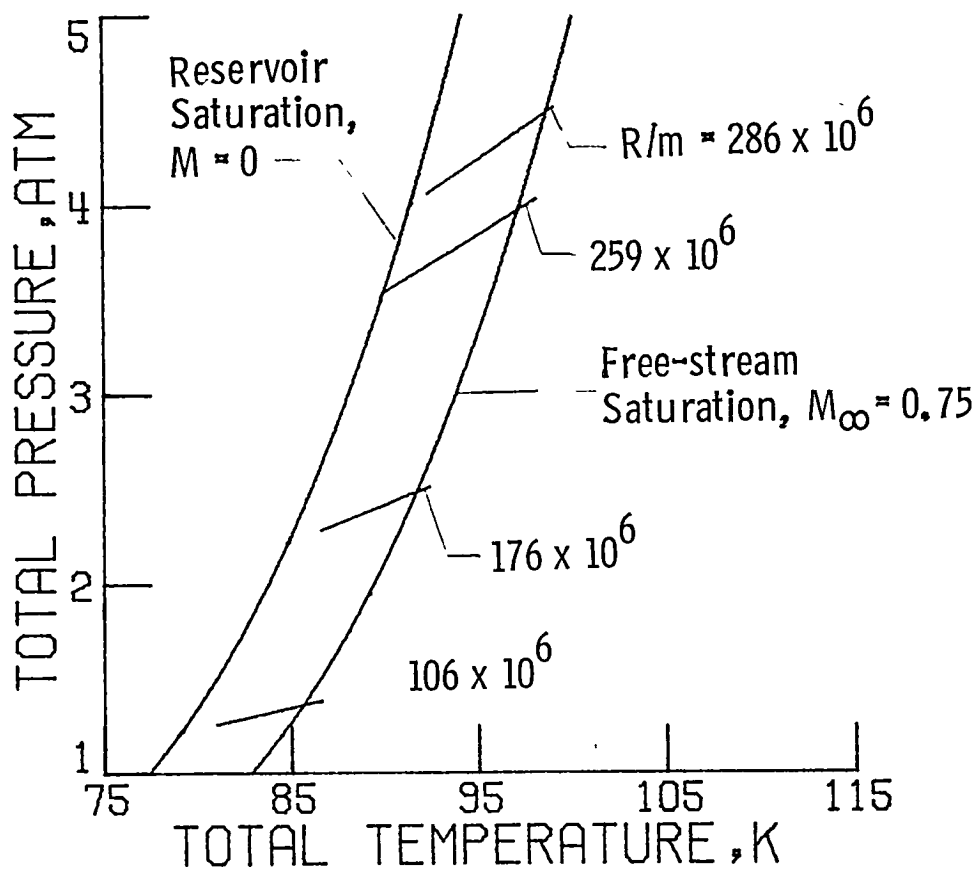
Figure 10.-- Paths at constant unit Reynolds number for the $M_\infty = 0.75$ test.
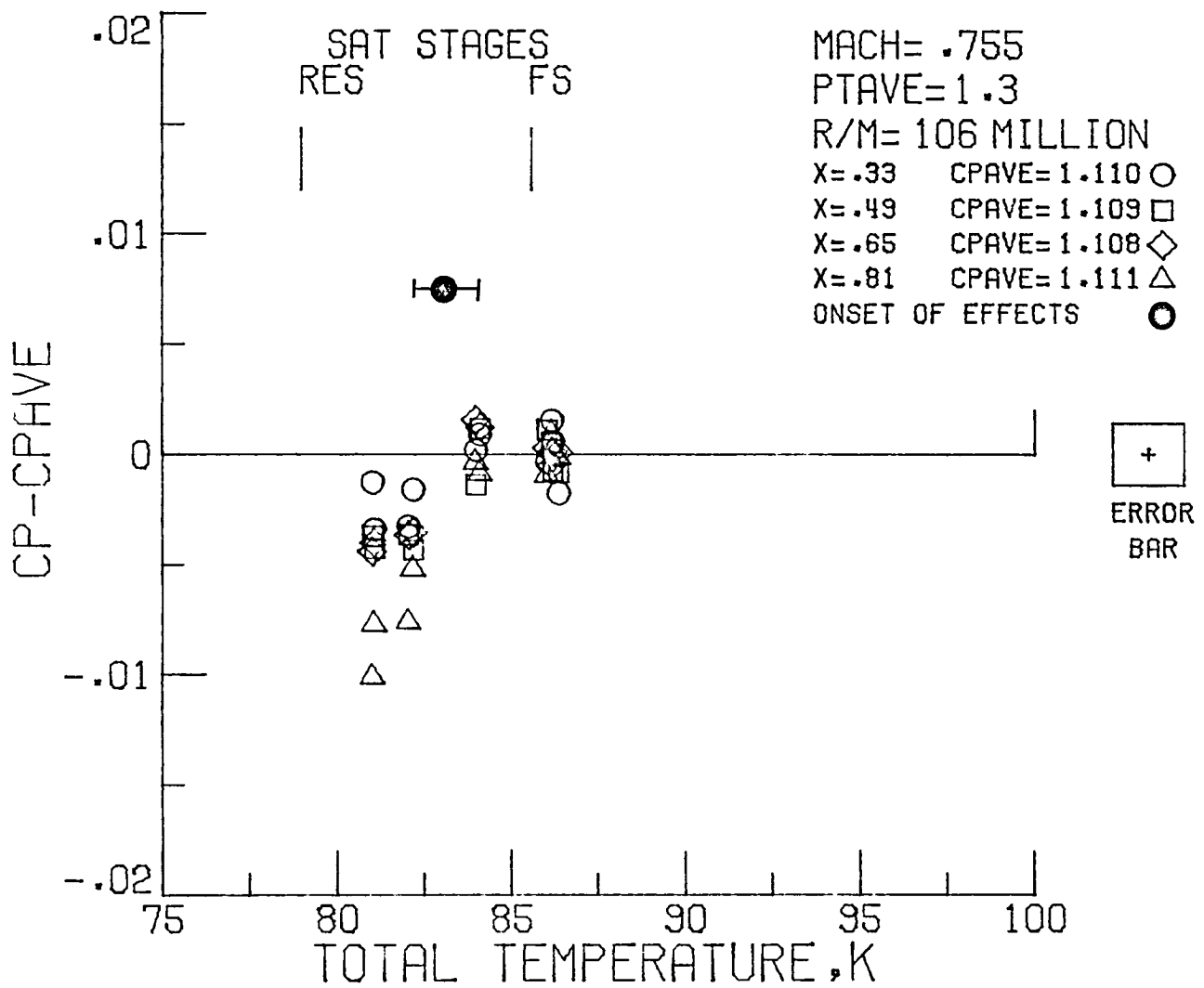
Figure 11.– Onset of condensation effects for the R/m = 106 x 10^6 path of the M_∞ = 0.75 test.
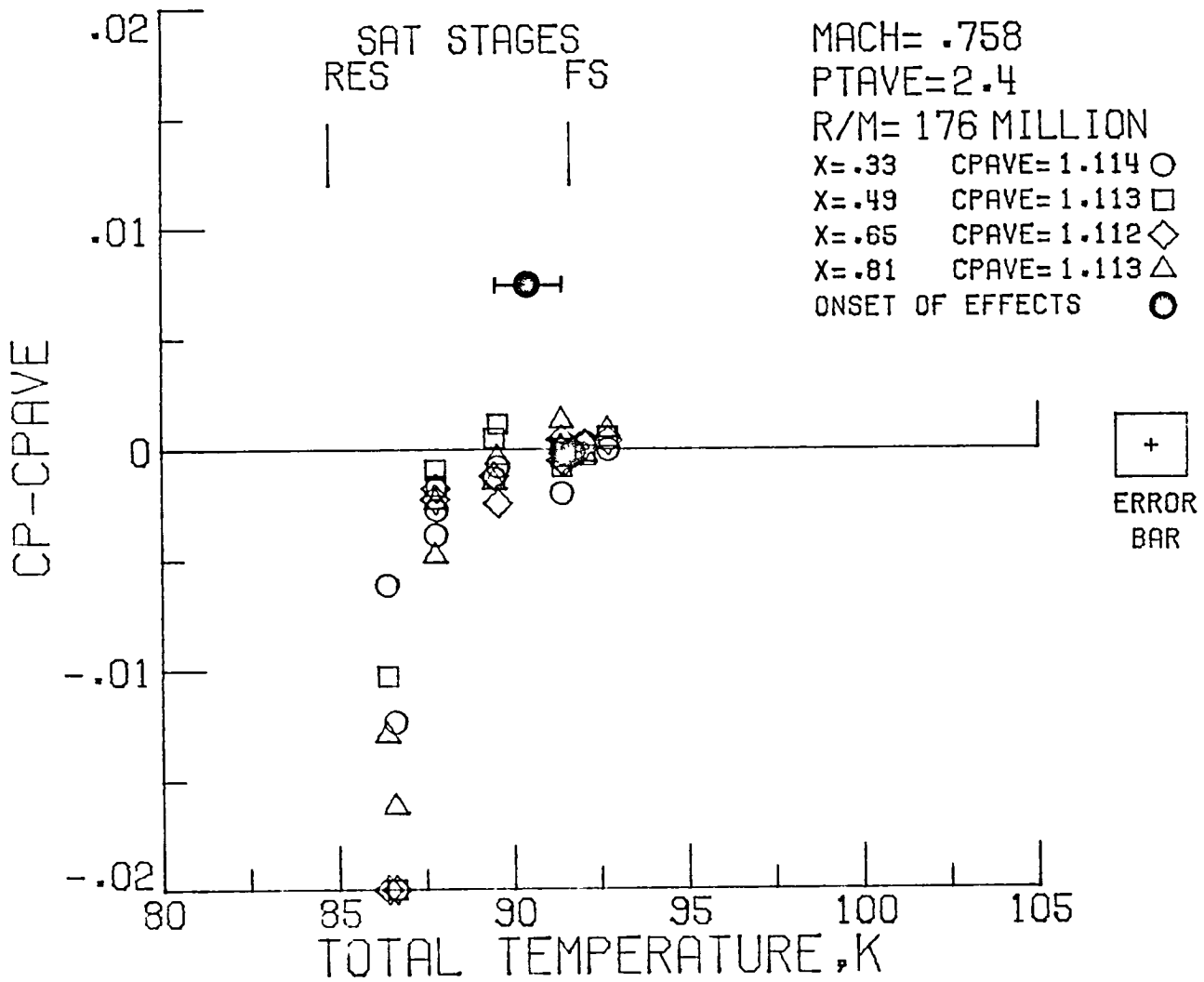
Figure 12.- Onset of condensation effects for the R/m = 176 x 10^6 path of the M$_\infty$ = 0.75 test.
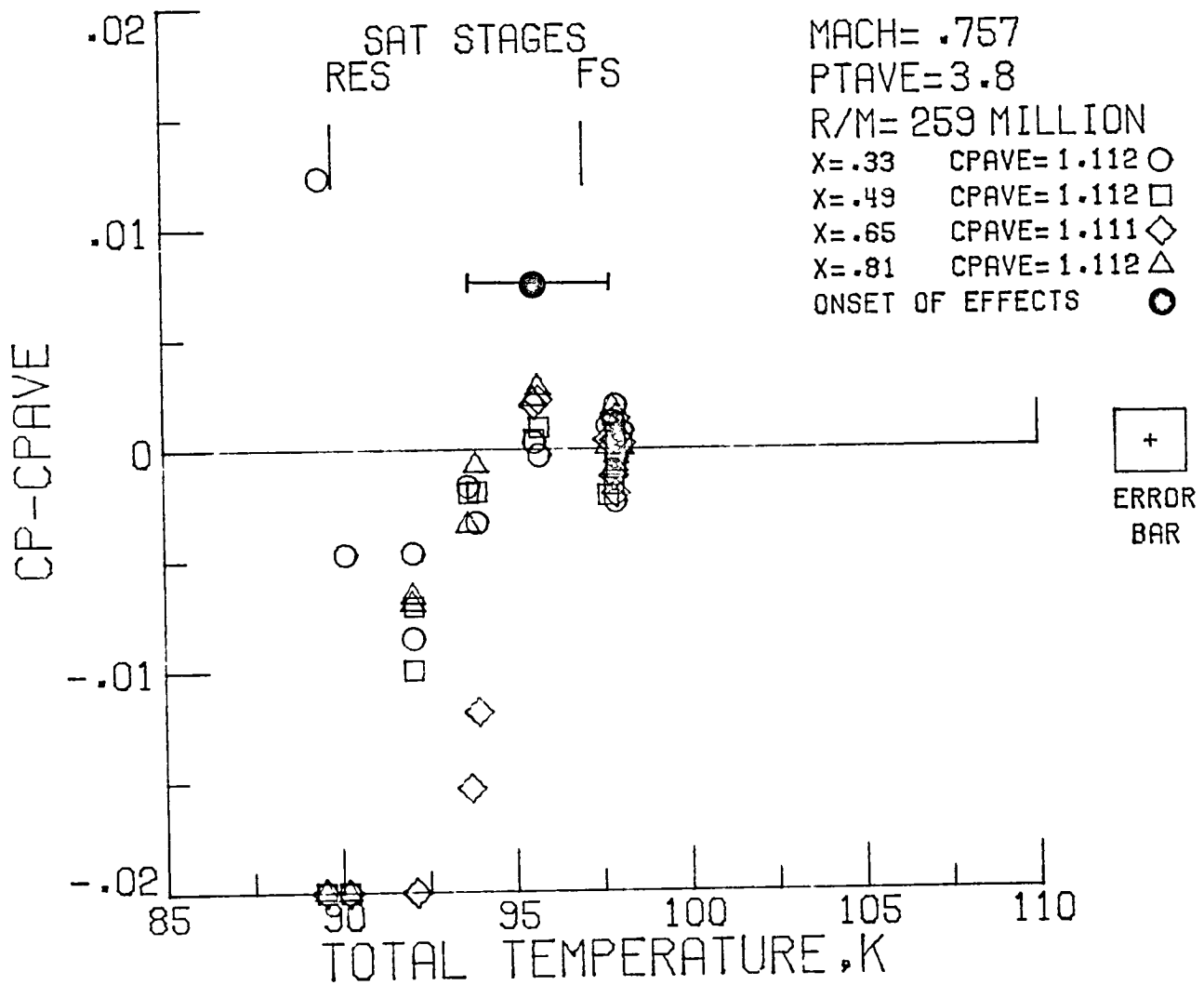
Figure 13.— Onset of condensation effects for the R/m = 259 x 10^6 path of the M_∞ = 0.75 test.

Figure 14. – Onset of condensation effects for the R/m = 286 x 10^6 path of the M$_\infty$ = 0.75 test.
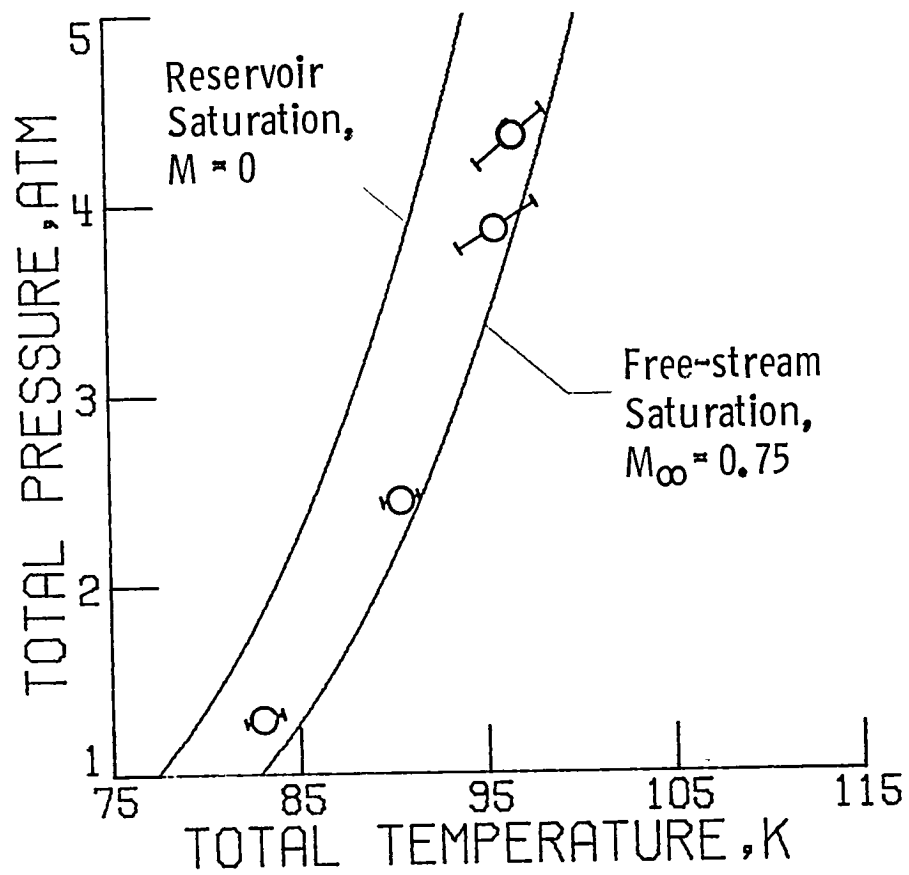
Figure 15.- Summary of the onset of condensation effects and the estimated uncertainties for the $M_{\infty} = 0.75$ test.
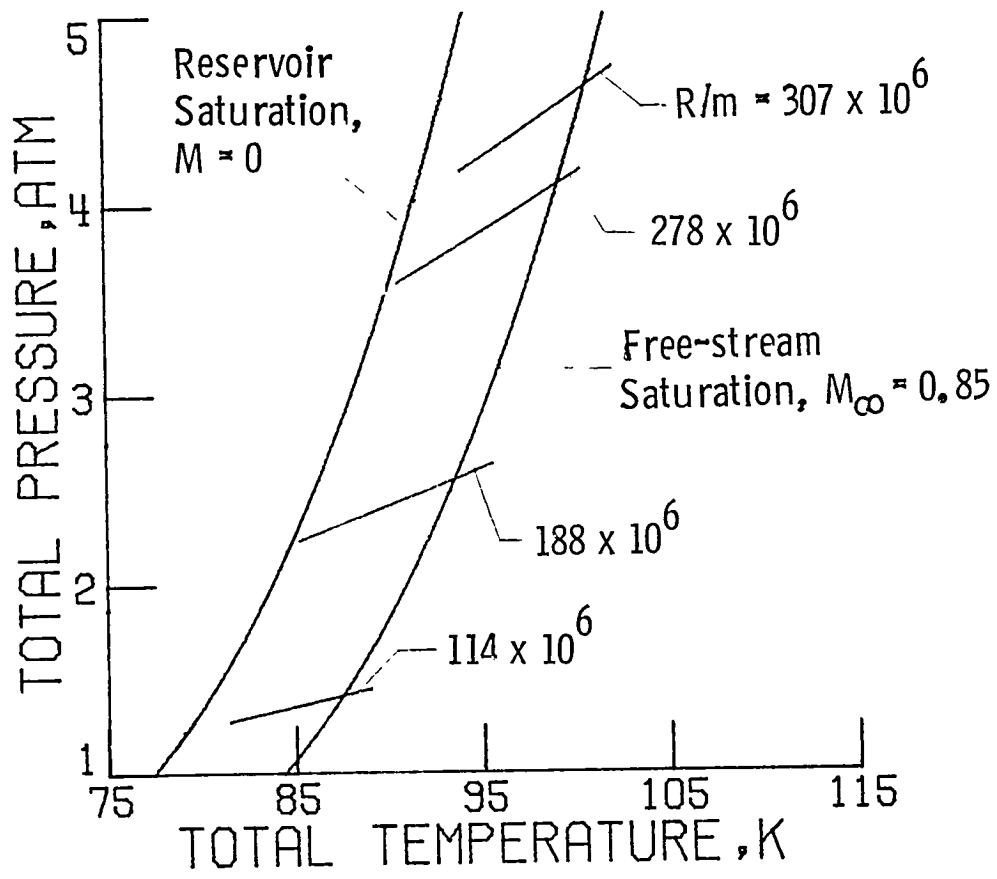
Figure 16.- Paths of constant unit Reynolds number for the $M_\infty = 0.85$ test.
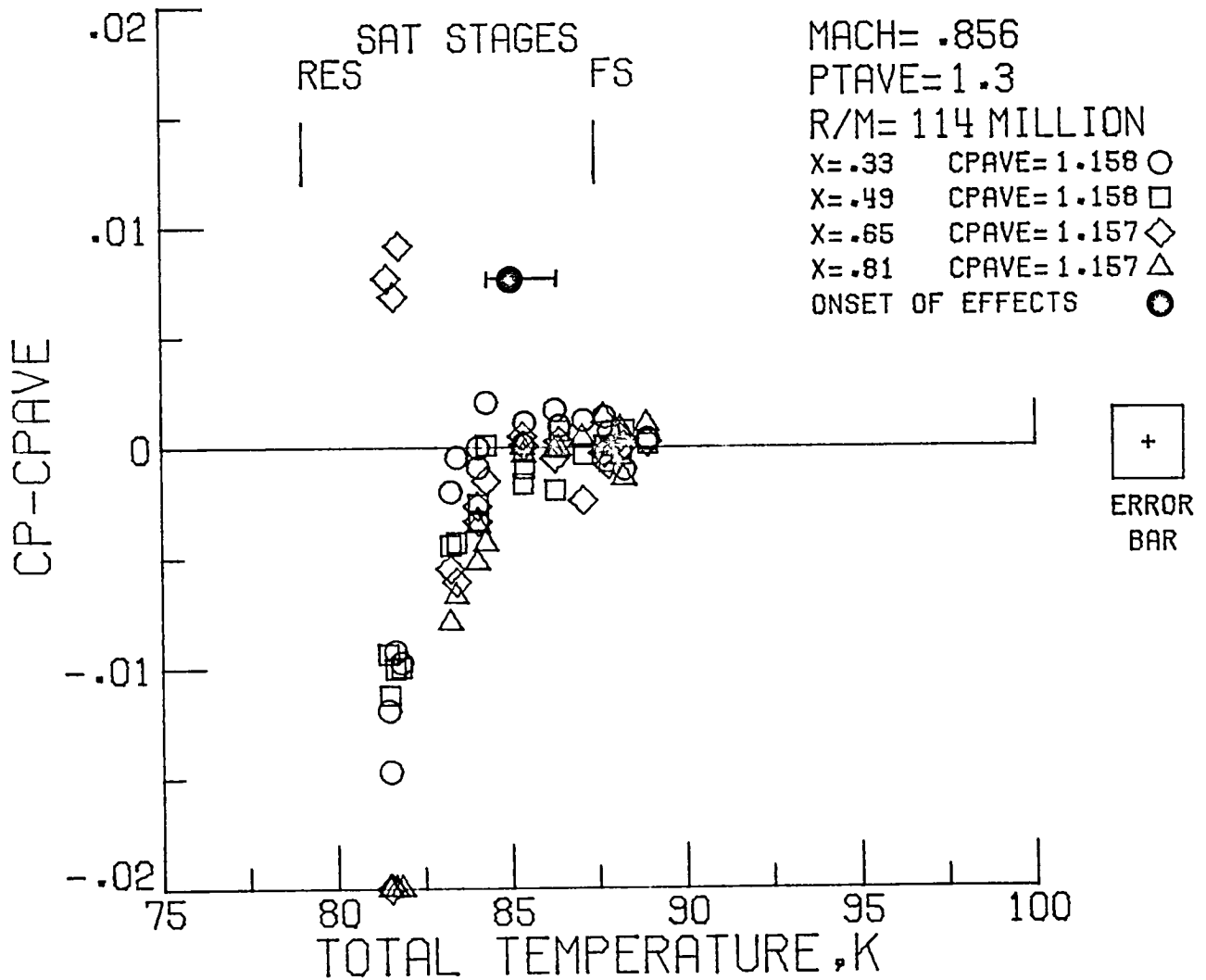
Figure 17.- Onset of condensation effects for the R/m = 114 x 10^6 path of the M_∞ = 0.85 test.
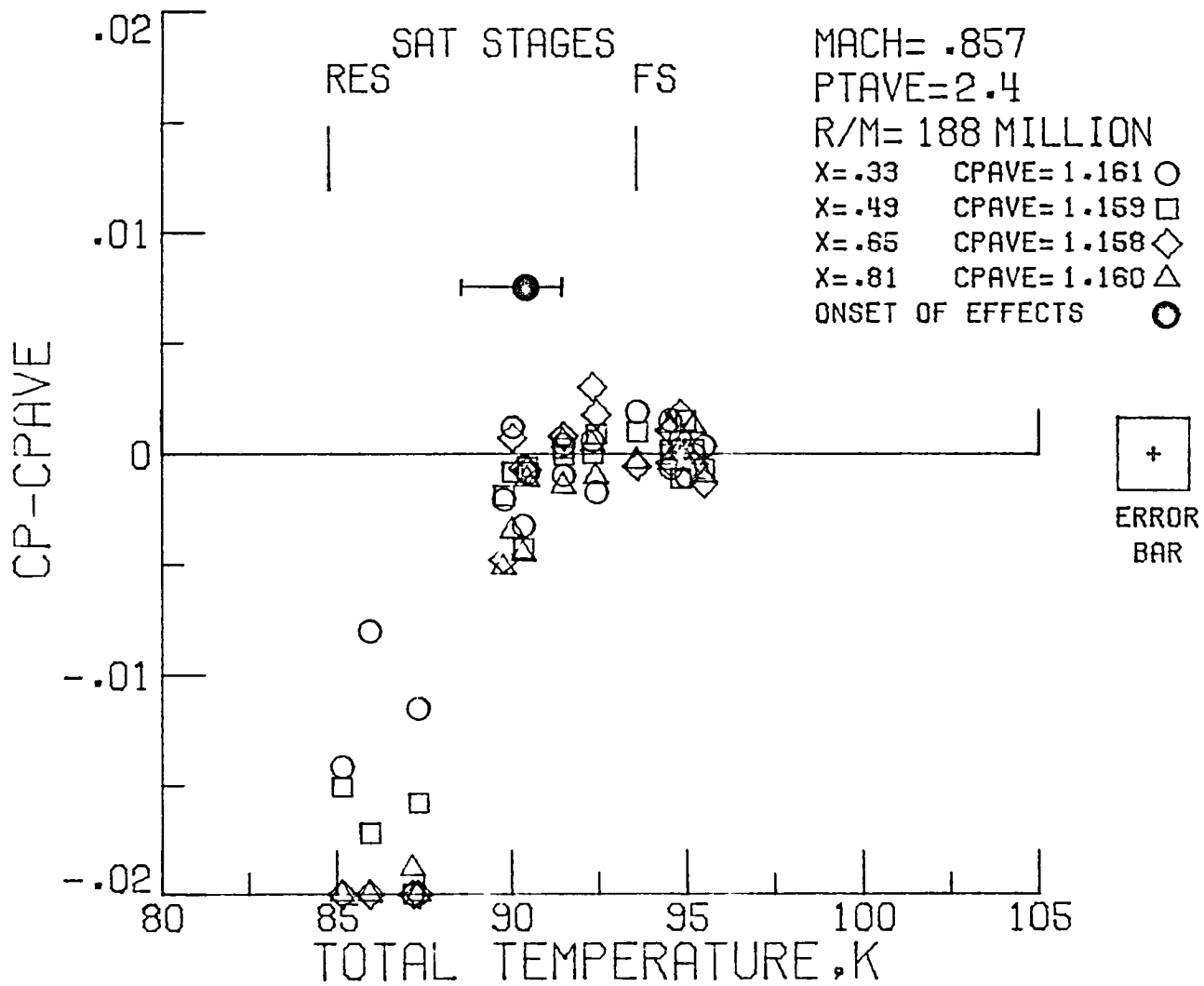
Figure 18. - Onset of condensation effects for the R/m $= 188 \times 10^6$ path of the $M_\infty = 0.85$ test.
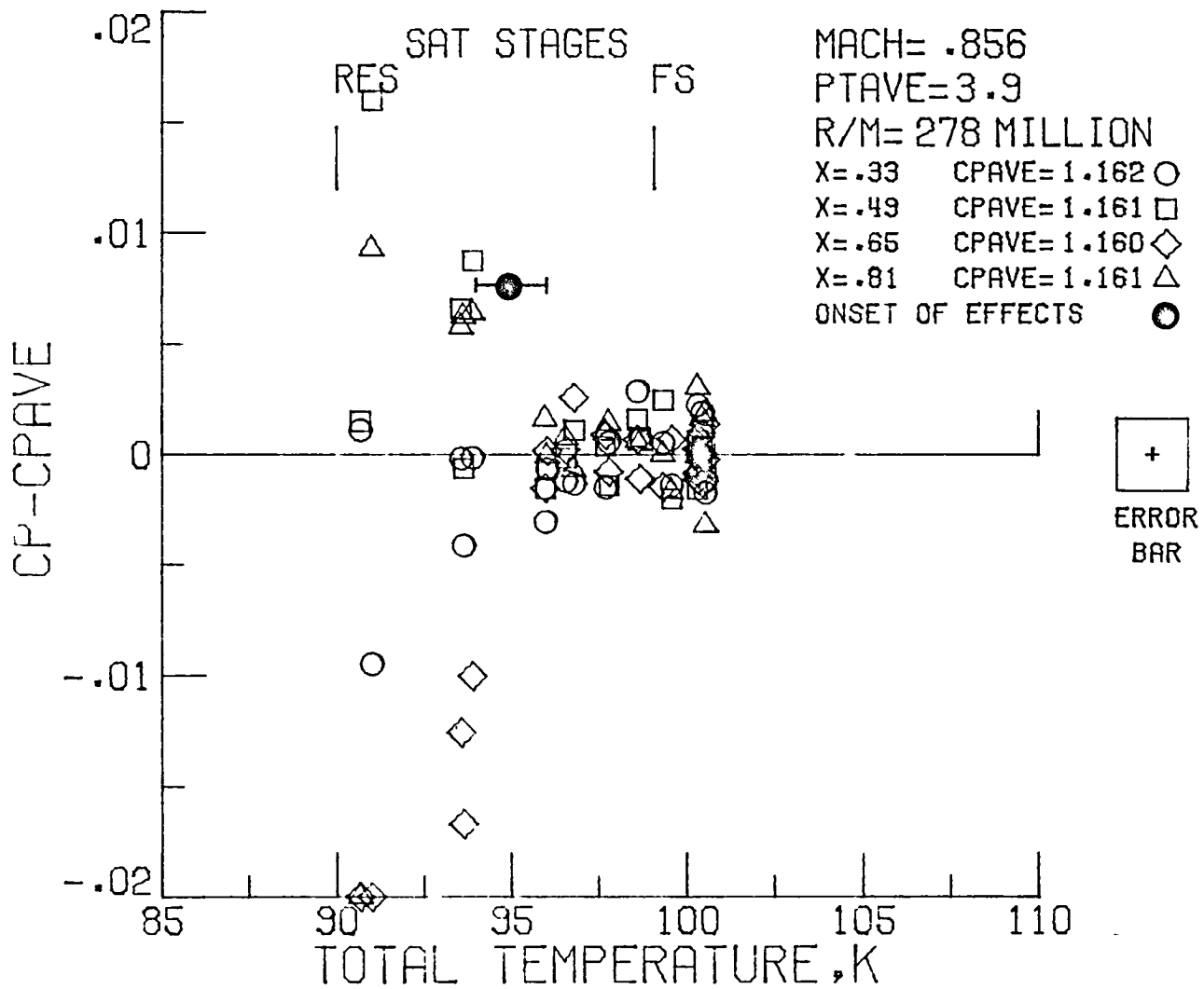
Figure 19.- Onset of condensation effects for the R/m = 278 x 10^6 path of the M_∞ = 0.85 test.
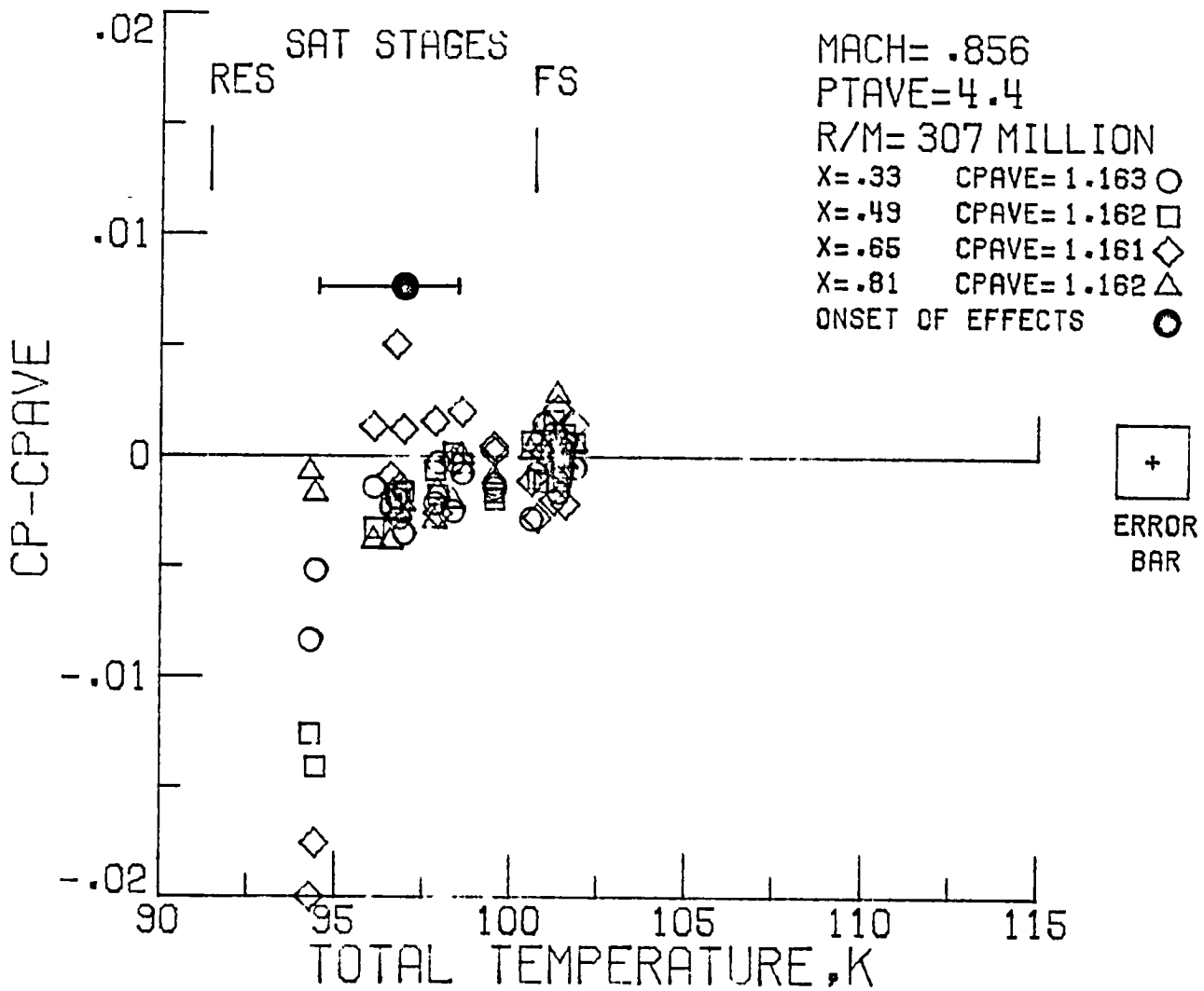
Figure 20. - Onset of condensation effects for the R/m = 307 x 10⁶ path of the M_∞ = 0.85 test.
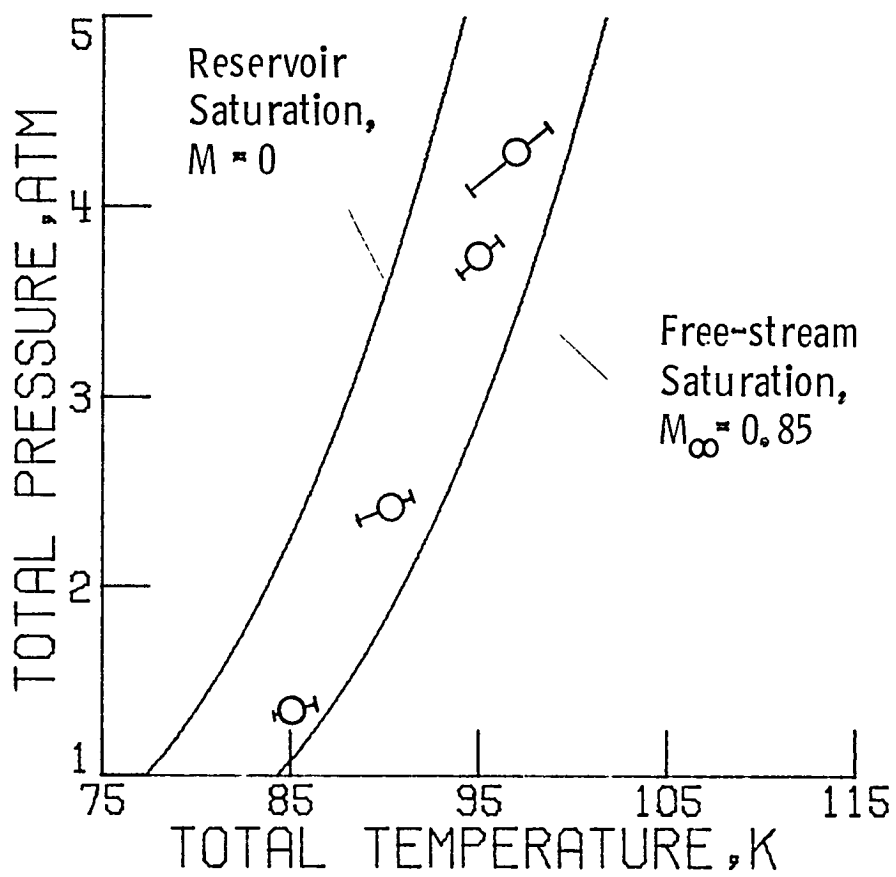
Figure 21.- Summary of the onset of condensation effects and the estimated uncertainties for the $M_\infty = 0.85$ test.
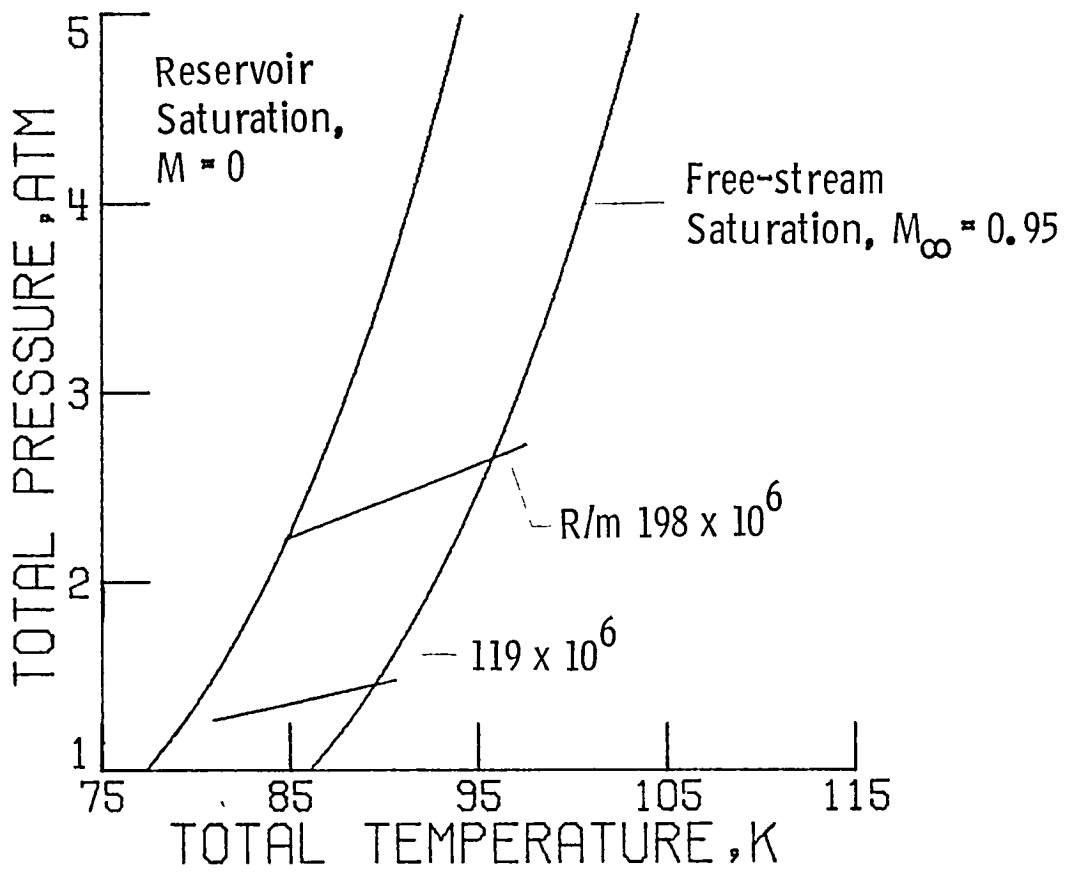
Figure 22.- Paths of constant unit Reynolds number for the $M_\infty = 0.95$ test.
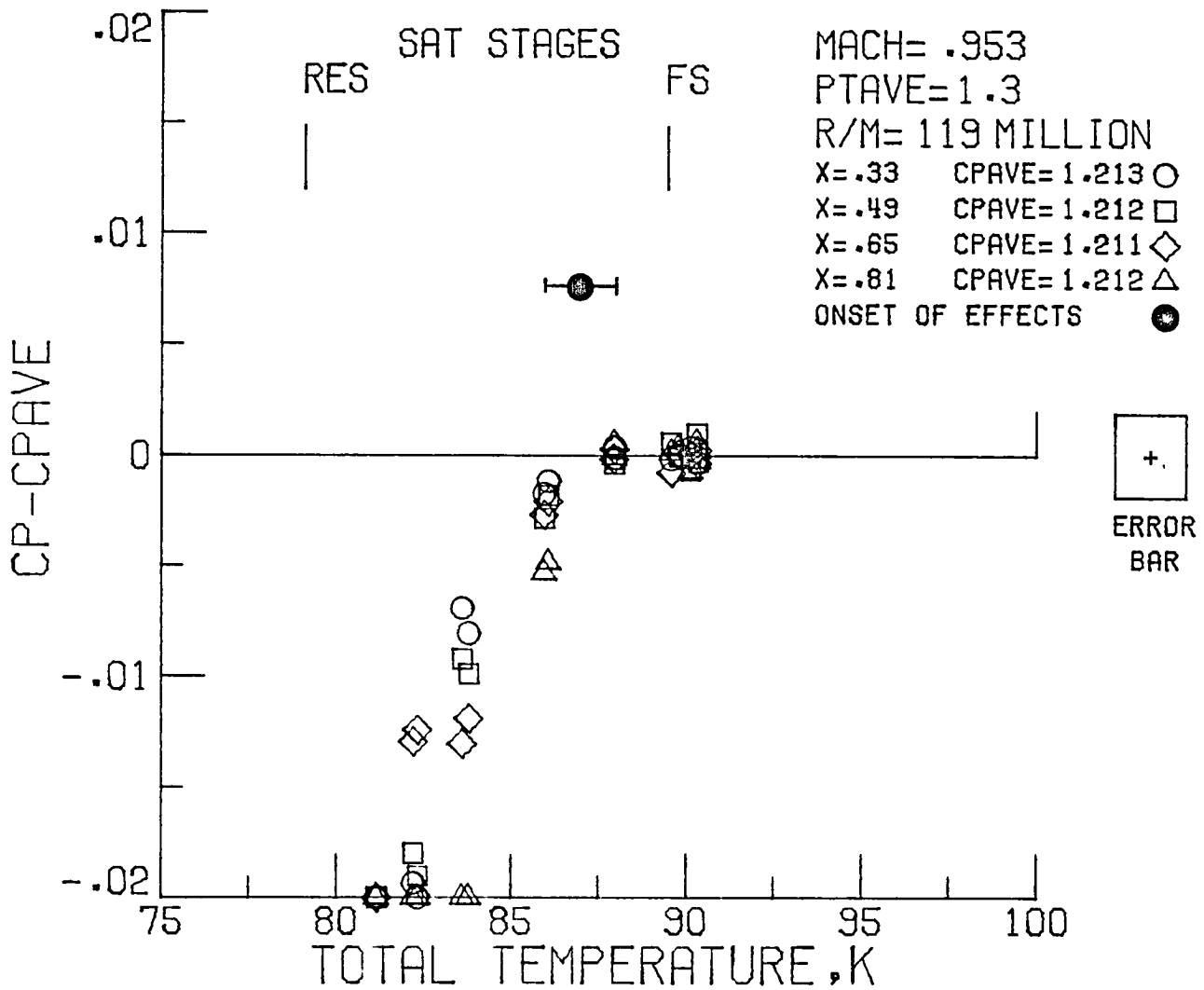
Figure 23. - Onset of condensation effects for the R/m = 119 x 10^6 path of the M_∞ = 0.95 test.
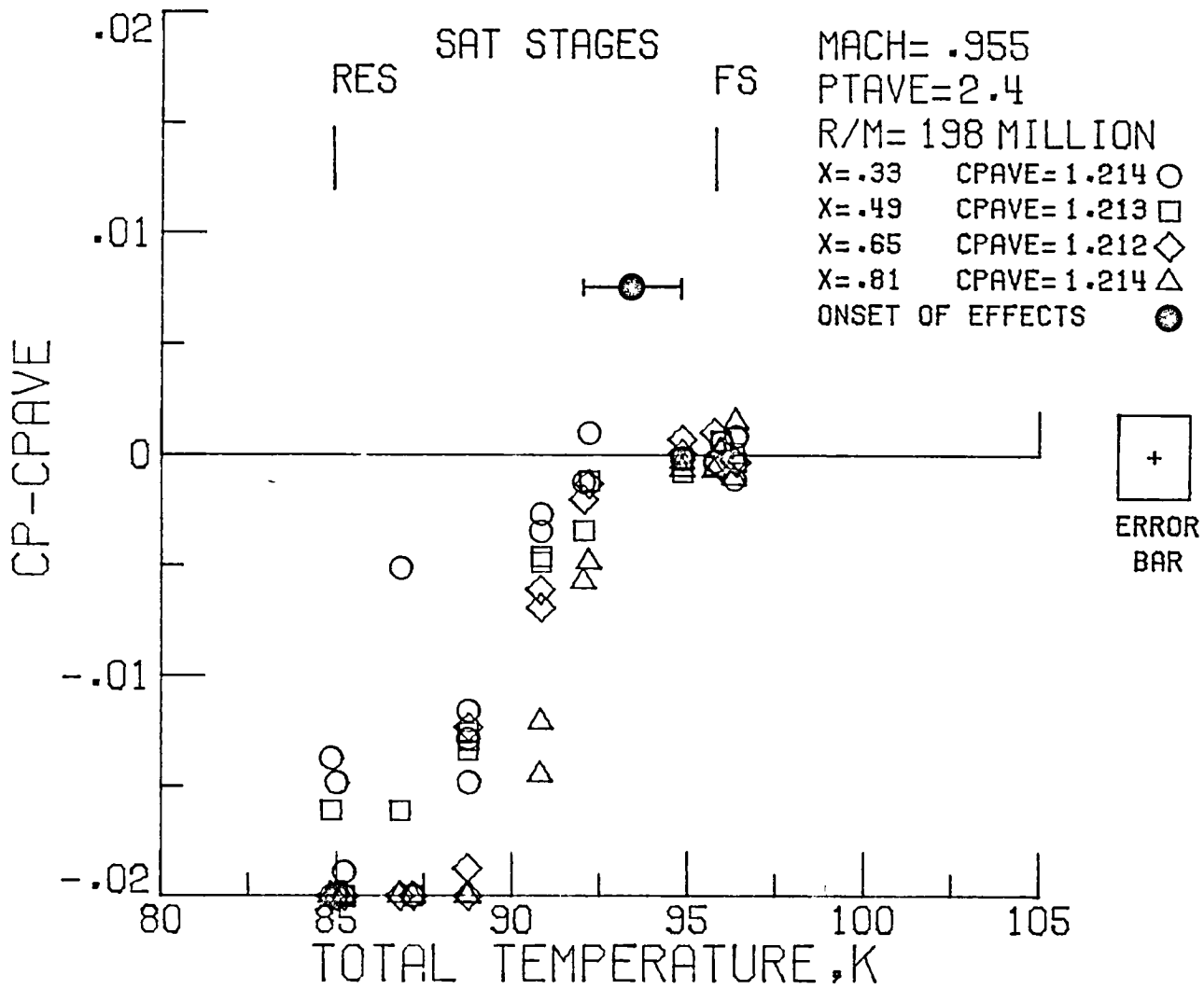
Figure 24. – Onset of condensation effects for the R/m = 198 x 10^6 path of the M_∞ = 0.95 test.
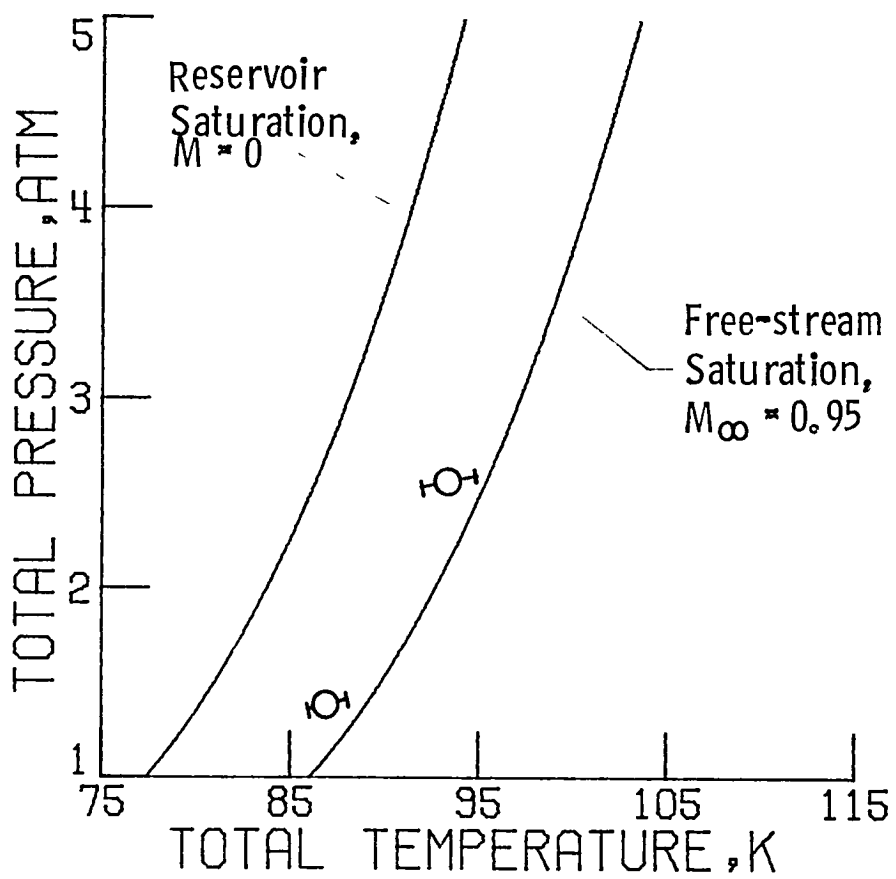
Figure 25. - Summary of the onset of condensation effects and the estimated uncertainties for the $M_\infty = 0.95$ test.
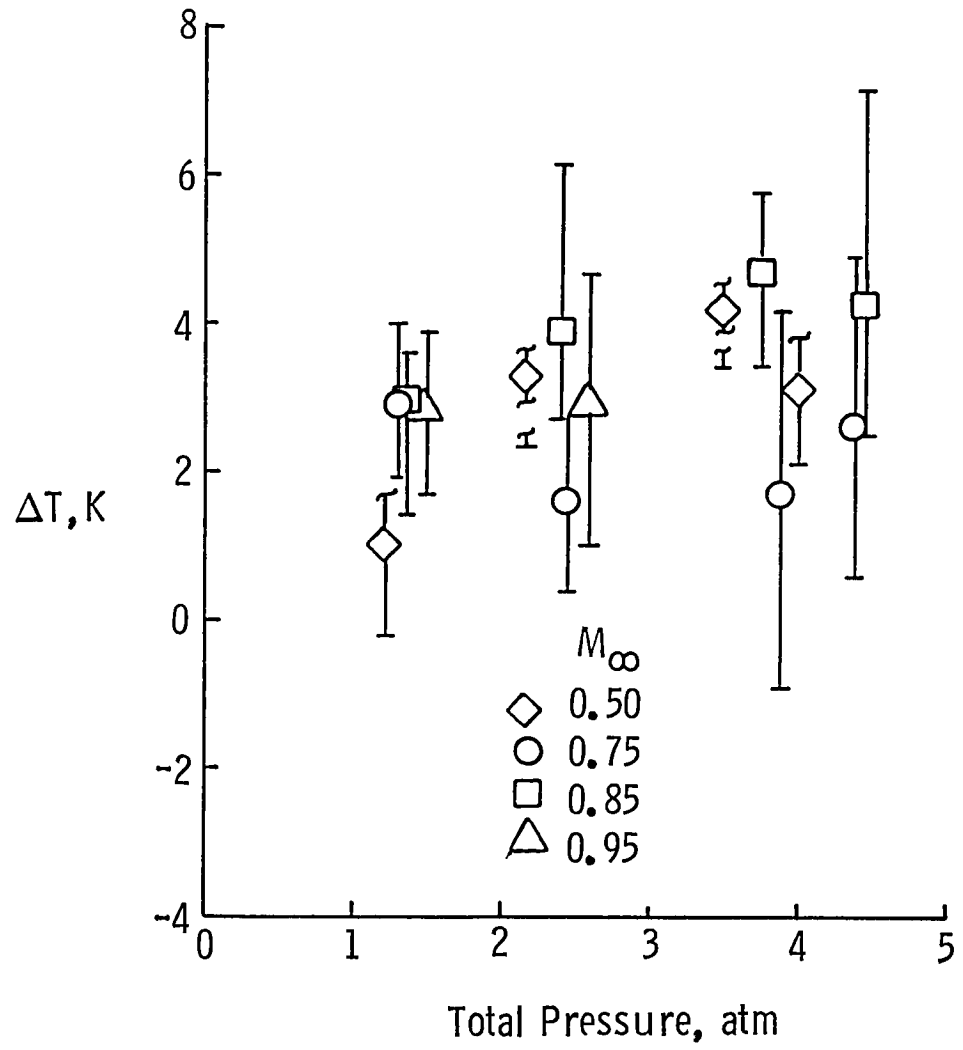
Figure 26.- Supercooling of total pressure probes based on M_∞ as a function of total pressure at onset.
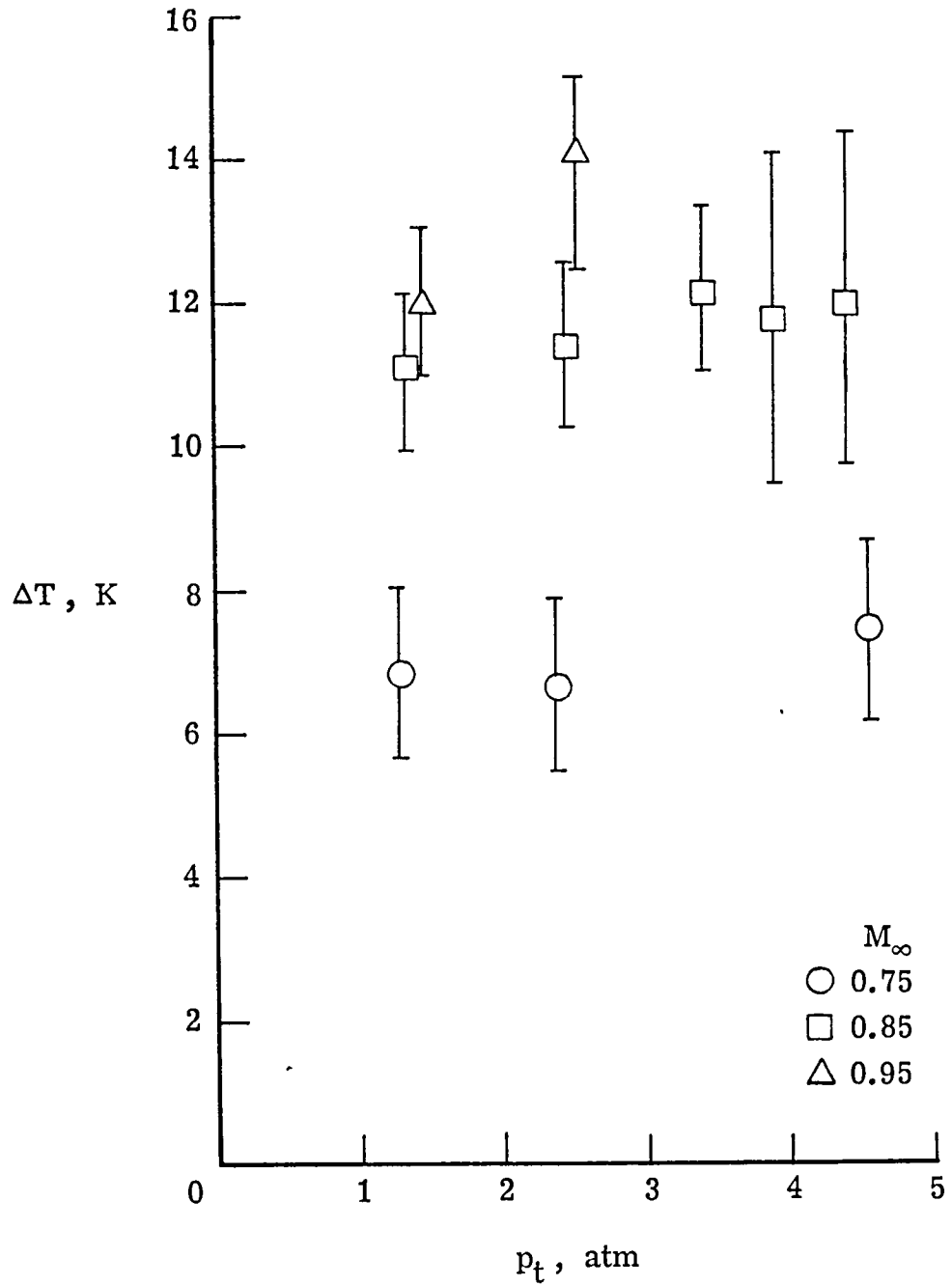
Figure 27.— Supercooling based on maximum local Mach number for the airfoil experiments of reference 2.
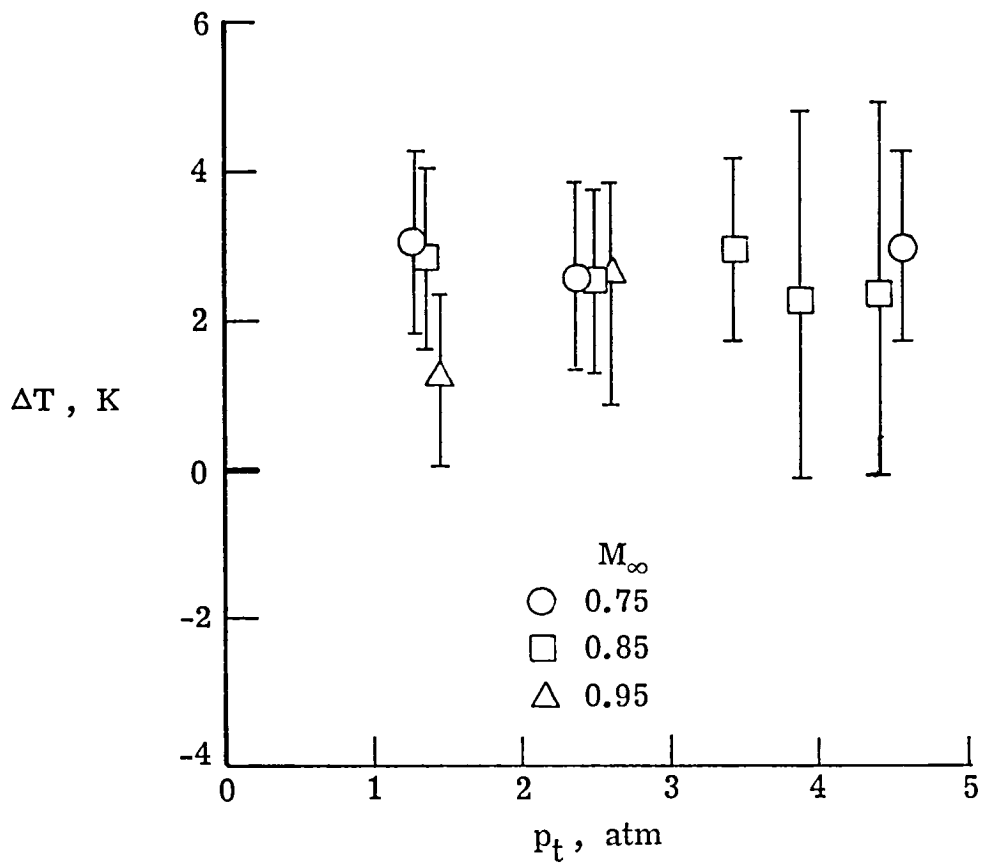
Figure 28. - Supercooling based on M_∞ for the airfoil experiments of reference 2.
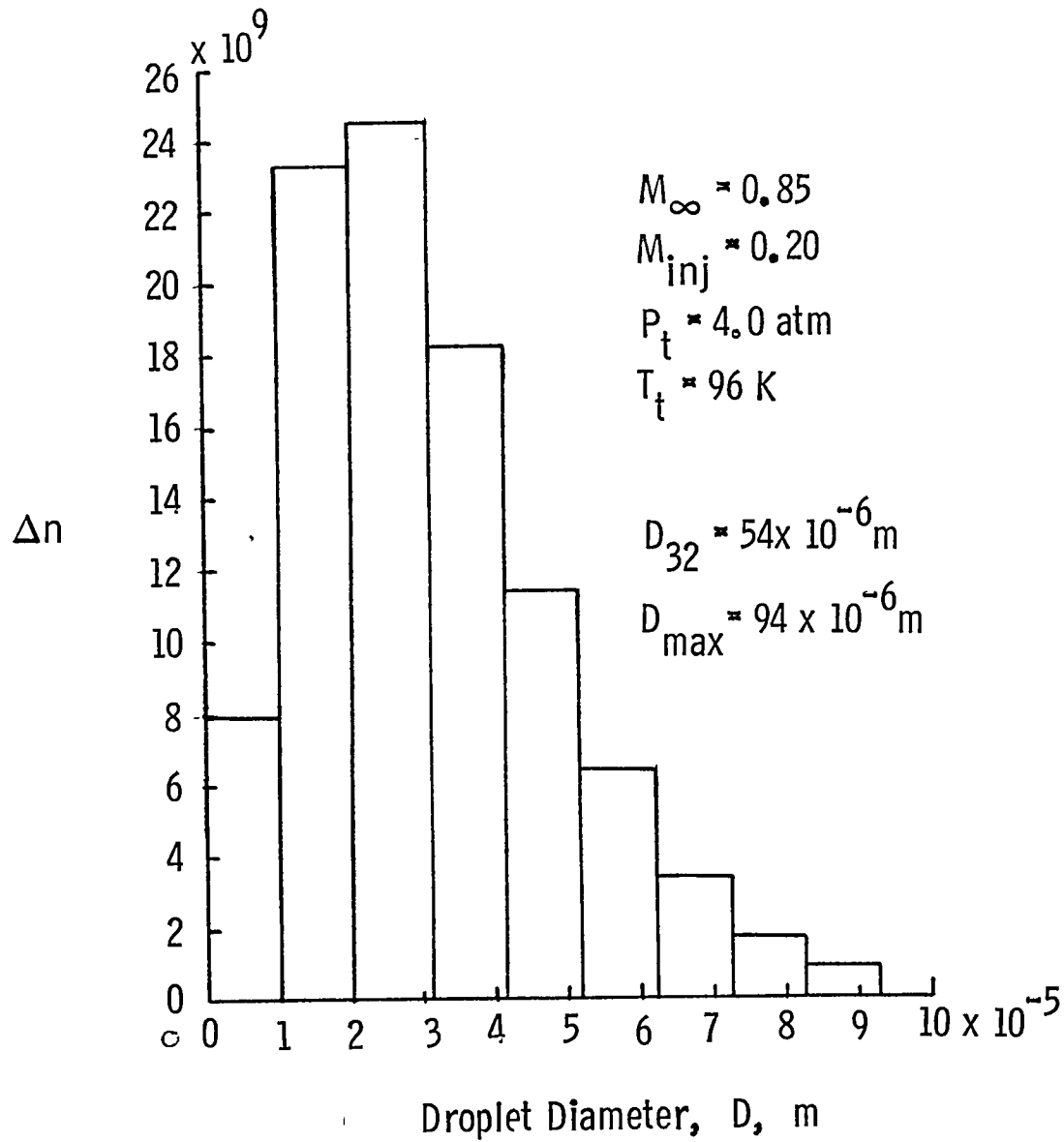
Figure 29. - Droplet distribution as predicted by Nukiyama-Tanasawa for cryogenic tunnel conditions typical of onset conditions. Ratio of liquid injected to test section mass flow is 0.0157.

End of Document